

THE (IN)STABILITY OF PLANETARY SYSTEMS

RORY BARNES AND THOMAS QUINN

Dept. of Astronomy, University of Washington, Box 351580, Seattle, WA, 98195-1580

E-mail: rory@astro.washington.edu, trq@astro.washington.edu

Draft version January 18, 2022

ABSTRACT

We present results of numerical simulations which examine the dynamical stability of known planetary systems, a star with two or more planets. First we vary the initial conditions of each system based on observational data. We then determine regions of phase space which produce stable planetary configurations. For each system we perform $1000 \sim 10^6$ year integrations. We examine ν And, HD83443, GJ876, HD82943, 47UMa, HD168443, and the solar system. We find that the resonant systems, 2 planets in a first order mean motion resonance, (HD82943 and GJ876) have very narrow zones of stability. The interacting systems, not in first order resonance, but able to perturb each other (ν And, 47UMa, and SS) have broad regions of stability. The separated systems, 2 planets beyond 10:1 resonance, (we only examine HD83443 and HD168443) are fully stable. Furthermore we find that the best fits to the interacting and resonant systems place them very close to unstable regions. The boundary in phase space between stability and instability depends strongly on the eccentricities, and (if applicable) the proximity of the system to perfect resonance. In addition to 10^6 year integrations, we also examined stability on $\sim 10^8$ year timescales. For each system we ran ~ 10 long term simulations, and find that the Keplerian fits to these systems all contain configurations which may be regular on this timescale.

1. INTRODUCTION

By September 2003, 13 planetary systems had been discovered (including our own Solar System). The extra-solar planetary systems (ESPS) are, possibly due to observational biases, markedly different from our own in several ways. In our solar system (SS) the Jovian mass planets all orbit at distances larger than 5AU, and on nearly circular orbits ($e \lesssim 0.05$). ESPS, on the other hand, contain giant planets in a wide range of distances and eccentricities; some are 10 times closer to their primary than Mercury, and others orbit with eccentricities larger than 0.5. In this paper we attempt to categorize these systems dynamically, constrain the errors of the orbital parameters, compare our SS to ESPS, explore the long term stability of each planetary system, and determine the mechanism(s) that maintain stability.

We examine these systems through numerical simulations. The integrations begin with slightly different initial conditions in order to probe observationally allowed configurations. This exploration of parameter space permits a quantitative measure of the stability of each system, and, hence, predicts which distribution of orbital elements will most likely result in a stable system. In addition, a comparison of stability between systems may reveal which elements are most critical to the stability of planetary systems in general.

A quick inspection of the known systems reveals three obvious morphological classifications: resonant, interacting, and separated. Resonant systems contain two planets that occupy orbits very close to a 2:1 mean motion resonance. A 3:1 system, 55Cnc (Marcy *et al.* 2002), has been announced, but its dynamics will not be examined here. Interacting systems contain planets which are not in mean motion resonance, but are separated by less than a 10:1 ratio in orbital period. These systems are not dynamically locked, but the planets perturb each other. The SS falls into this category. The final classification is

systems in which the (detected) planets' orbits are beyond the 10:1 resonance. These planets are most likely dynamically decoupled, however some of these systems warrant investigation.

We examine planetary systems on two different timescales. First, we explore parameter space in 10^6 year integrations. For these simulations we vary initial conditions to determine stable regions within the observed errors. Second, we continue several stable simulations for an additional 10^8 - 10^9 years. From these runs we then learn how robust the predicted stable regions are, and we also determine the mechanisms that lead to stability. Specifically we evaluate the hypothesis that some stable system require secular resonance locking.

In many ways this paper performs the direct analysis that is approximated by MEGNO (Cincotta & Simó 2000, see also Robutel & Laskar 2001, Michtchenko & Ferraz-Mello 2001, and Goździewski 2002). MEGNO searches parameter space for chaotic and periodic regions. Our simulations show that to first order MEGNO's results do uncover unstable regions. In general, however, chaotic systems can be stable for at least 10^9 years, as shown below. Our SS also shows chaos on all timescales (for a complete review, see Lecar, *et al.* 2001), therefore only direct N-body integration can determine stability.

This work represents the largest coherent study of planetary system dynamics to date. Our simulations show that the true configurations of most planetary systems are constrained by just a few orbital elements (or ratios of elements), and that stable regions can be identified with integrations on the order of 10^6 years. We also find that stability, as well as constraints on stability, are correlated with morphology. Resonant system stability depends strongly on the ratio of the periods, interacting systems on eccentricities, and separated systems are stable.

This paper is structured as follows. In §2 we describe the generation of initial conditions, integration technique, and introduce the concept of a stability map. In §3 we analyze the results of the resonant systems HD82943 and GJ876. In §4

we examine the interacting systems of 47UMa, ν And, and the SS. In §5 the separated systems, specifically HD168443 and HD83443, are discussed briefly. In §6 we summarize the results of §3-5, In §7 we discuss possible formation scenarios and inconsistencies between this work and other work on planetary systems. Finally in §8 we draw general conclusions, and suggest directions for future work.

2. NUMERICAL METHODS

In this section we outline the techniques used to perform and analyze these simulations. This paper follows the example of Barnes and Quinn (2001, hereafter Paper I). First we describe how the initial conditions of each of the short term simulations are determined. In §2.2 we describe our integration method. Finally in §2.3 we describe a convenient way to visualize the results of these simulations, the stability map.

2.1. Initial Conditions

In order to explore all of parameter space we must vary 5 orbital elements, (the period P , the eccentricity e , the longitude of ascending node Ω , the longitude of periastron, ϖ , and the inclination i) and every mass in the system. The period and the semi-major axis a are related by Kepler's third law. The argument of pericenter, ω is the difference ϖ and Ω .

For each system we perform 1000 simulations, each with different initial conditions. Orbital elements that are easily determined via the Doppler method (P.e. ϖ) are varied about a Gaussian centered on the nominal value, with a standard deviation equal to the published error. We do not permit any element to be more than 5σ from the mean. For the i and Ω elements, flat distributions in the ranges $0^\circ < i < 5^\circ$ and $0 < \Omega < 2\pi$ were used. Note that this distribution of i and Ω permits a maximum mutual inclination of 10° . These randomized orbital elements are relative to the fundamental plane.

The Doppler method of detection does not produce a normal error distribution. As Konacki & Maciejewski (1999) show, the error in eccentricity can have a large tail toward unity. However their method, or other statistical methods, such as bootstrapping, require all the observational data (including reflex velocity errors) to determine the shape of this error curve. As not all the observations of multiplanet systems have been published we are forced to use a normal distribution in order for comparison between systems to be meaningful. We therefore encourage all the observational data to be published, as some of the results presented here (specifically comparing the percentage of simulations that survived) are less meaningful because we are unable to accurately estimate the error distributions of the orbital elements. For completeness we also vary the primaries' masses, M_* , based on other observations (generally determined via spectral fitting). However as the stars are all at least 100 times more massive than their planetary companions, the slight variations in primary mass should not affect stability.

The masses of the planets are determined by the following relation

$$m = \frac{m_{obs}}{|\sin(\cos^{-1}(\sin i)\cos\Omega)|} \quad (1)$$

where m is the true mass of the planet, and m_{obs} is the observed minimum mass. By varying the mass this way, we account for all possible orientations, and connect the inclination of the system in its fundamental plane, to its inclination in the sky. Note

that this scheme requires the azimuthal angles in the planetary systems to be measured from the line of sight.

2.2. Integration

With initial conditions determined the systems were then integrated with the RMVS3 code from the SWIFT suite of programs¹(Levison & Duncan 1994). This code uses a symplectic integration scheme to minimize long term errors, as well as regularization to handle close approaches. The initial timestep, Δt is approximately 1/30th of the orbital time of the innermost planet. In order to verify the accuracy of the integrations, the maximum change in energy, ϵ , permitted was 10^{-4} . We define ϵ as

$$\epsilon = \frac{\max|E_i - E_0|}{E_0}, \quad (2)$$

where E_i represents an individual measurement of the energy during the simulation, and E_0 is the energy at time 0. There are two reasons for using this threshold in ϵ . First, as the integration scheme is symplectic, no long term secular changes will occur, so high precision is not required. Second, the simulations needed to be completed in a timely manner. If a simulation did not meet this energy conservation criterion, it was rerun with the timestep reduced by a factor of 10. The minimum timestep we used was $P_{inner}/3000$. Despite this small timestep, a few simulations did not conserve energy, and were discarded, except that they were incorporated into the errors. Errors and error bars include information from unconserved simulations. Simulations which fail to conserve energy would most likely be labeled as unstable, as the failure of energy conservation undoubtedly results from a close encounter between two bodies, which usually results in an ejection. Therefore the estimates for stability in the systems presented here should be considered *upper limits*.

Throughout this paper we adopt the nomenclature of the discovery papers (planets have been labeled b, c, d, etc, with order in the alphabet corresponding to order of discovery). We will also introduce another scheme based on mass. Planets will be subscripted with a 1, 2, 3, etc, in order of descending mass. This new scheme is more useful in discussing the dynamics of the system.

The short term simulations are integrated until one of the following criteria is met. 1) The simulation ejects a planet. Ejection is defined as the osculating eccentricity of one planet reaching, or exceeding unity. 2) The simulation integrates to completion at time τ . For these simulations, τ is defined as

$$\tau \equiv 2.8 \times 10^5 P_1, \quad (3)$$

or 280,000 times the period of the most massive planet. This choice corresponds to 10^6 years for the ν And system, as was simulated in Paper I.

If a system ends without ejection, then the stability of the system must be determined. There are several possible definitions of stability. In Paper I, a system was stable if the osculating eccentricity of each companion remained below 1 for the duration of the simulation. The most obvious flaw in this definition is that a planet could suffer a close approach and be thrown out to a bound orbit at some arbitrarily large distance. Such a system would bear no resemblance to the observed system, and hence should be labeled unstable. Here we adopt a more stringent definition, namely that the semi-major axes of all companions cannot change by more than a factor of 2. Changes in semi-major

¹SWIFT is publicly available at <http://k2.space.swri.edu/~hal/swift.html>

axis represent a major perturbation to the system, therefore this second cut is conservative, and only eliminates systems which expel a planet to large distances without fully ejecting it.

In addition to these short term simulations, we completed simulations to explore longer term stability ($\sim 10^8$ yrs). For each system we ran ~ 10 simulations, chosen to cover a wide range of stable parameter space. For these runs we started with the final conditions of stable configurations and continued them. These simulations therefore give us a handle on how the system is likely to evolve on timescales closer to its age ($\sim 10^9$ yrs). Those systems which survived these longer runs are the best comparisons to the true system. Hence they are the best simulations for determining the factors that lead to planetary system stability.

There are two notable problems with this methodology. First, we ignore the effects of general relativity, which may be important in some systems, specifically GJ876, and ν And. General relativity was included in our treatment of ν And in Paper I. In Paper I, the innermost planet had a negligible effect on the system, and we presume that general relativity will continue to be unimportant for the systems studied here. Second, we treat all particles as point masses. This is again especially troublesome for GJ876 and ν And, because of their proximity to their (presumably) oblate primaries. The sphericity of the stars also prohibits any tidal circularization of highly eccentric planets (Rasio *et al.* 1996). This may artificially maintain large planetary eccentricities, and increase the frequency of close encounters. However the eccentricities must become very large for this effect to become appreciable. We therefore assume that this phenomenon will not adversely affect our results. Ignoring these two issues should impact the results minimally while speeding up our simulations considerably.

2.3. Stability Maps

When analyzing the simulations, it is useful to visualize the results in a stability map. In general a stability map is a 3 dimensional representation of stability as a function of 2 parameters. In resonant systems, we find that several parameters determine stability. The most important is the ratios of the periods of the two resonant planets, which we will call R :

$$R \equiv \frac{P_{\text{outer}}}{P_{\text{inner}}}. \quad (4)$$

In coupled systems, e_1 and e_2 are the relevant parameters. The advantage to this visualization is that boundaries between stability and instability are easily identified.

The disadvantage of this form of visualization is that if the range of parameter space is not uniformly sampled (as it is here), we cannot visualize the errors. It is therefore important to bear this disadvantage in mind. At the edges of stability maps, the data are poorly sampled and the information at the edges should largely be ignored. To aid the visualization we have smoothed the maps. If a bin contained no data then it was given the weighted mean of all adjacent bins, including diagonal bins. This methodology can produce some misleading features in the stability maps. Most notable are tall spikes, or deep depressions in sparsely sampled regions. We comment on these types of errors where appropriate.

The procedure as outlined overestimates the size of stable regions in two important ways. First, the integration times are generally less than 0.1% of the systems' true ages. As is shown

throughout this paper, instability can arise at any timescale. Therefore, the stability zone will continue to shrink as the system evolves. Second we have chosen a very generous cut in semi-major axis space. Other studies permit Δa to be no larger than 10% (Chiang, Tabachnik, & Tremaine 2001). Lowering this variation would undoubtedly also constrict stability zones.

3. RESONANT SYSTEMS

Two systems with orbital periods in 2:1 mean motion resonance have been detected: HD82943² and GJ876 (Marcy *et al.* 2001a). Table 1 lists the orbital elements and errors for the resonant systems. For now we do not examine the 3:1 55Cnc system. The current best Keplerian fit to the observations put HD82943 and GJ876 just beyond perfect resonance. These planets all occupy high eccentricity orbits and hence have wide resonance zones. Simulations of these systems show that stability is highly correlated with the ratio of the periods, R , and to a lesser degree on e_1 . These systems are the least stable as less than 20% of simulations survived to τ .

3.1. HD82943

Two planets orbit the $1.05 \pm 0.05 M_{\odot}$ G0 star (Santos *et al.* 2000) HD82943 at semi-major axis distances of 0.73 and 1.16 AU. Planet b is the inner and less massive, c, the outer and more massive. Goździewski & Maciejewski (2001) also examined this system. They found that the system is most likely to be stable in perfect resonance. These simulations must run for 340,830 years, τ_{HD82943} . The long term simulations were run for 100 million years.

For this system we find that $18.8\% \pm 4.3\%$ of the trials were unperturbed to τ_{HD82943} , and 19.3% survived for 10^6 years, and 4.5% failed to conserve energy. Fig. 1 shows the instability rate to 10^6 years. Most unstable simulations break our stability criterion within 10^4 years, but others survived more than 900,000 years before being ejected. The asymptotic falloff to 10^6 years implies we have found most unstable configurations. In 91.3% of the trials, planet b, the inner and less massive planet, was ejected/perturbed. In order to check the simulations, Fig. 2 plots the rate of survival as a function of energy conservation. From this figure it appears that our limit of 10^{-4} is reasonable, as there appears to be no trend in stability as a function of energy conservation. The spike in survivability at 10^{-8} corresponds to regular orbits that were stable for our initial choice of Δt . The lack of a trend with energy conservation (specifically survival probability increasing with decreasing ϵ), implies our cutoff value of ϵ is stringent enough.

Stability in this system is correlated with R , e_c , ΔM and $\Delta \varpi$, where ΔM is the difference in mean anomaly, and $\Delta \varpi$ is the difference in initial longitude of periastron. Slightly beyond perfect resonance is the preferred state for this system. This system also requires the eccentricity of planet c to remain below 0.4. These features are shown in Figs. 3 and 4. In these greyscale images, black represents unsampled regions, darkest grey marks regions in which no configurations survived, grades of stability are denoted by lighter shades of grey, and white is fully stable. As with most stability maps in this paper, the outer 2-3 gridpoints should be ignored. In Fig. 3, the $R - e_c$ stability map, the large "plateau" at low e , is therefore poorly sampled, as is the island at $R=2.15$, $e_c=0.52$. The most striking feature of this figure is that the best fit to the system, the asterisk, places

²<http://obswww.unige.ch/~udry/planet/hd82943syst.html>

Table 1 - Initial Conditions for Resonant Systems

| System | Planet | Mass(M_J) | Period(d) | Eccentricity | Long. of Peri.(Deg) | Time of Peri. (JD) |
|---------|--------|---------------|------------------|-----------------|---------------------|----------------------|
| GJ876 | c | 0.56 | 30.12 ± 0.02 | 0.27 ± 0.04 | 330.0 ± 12.0 | 2450031.4 ± 1.2 |
| | b | 1.89 | 61.02 ± 0.03 | 0.10 ± 0.02 | 333.0 ± 12.0 | 2450045.2 ± 1.9 |
| HD82943 | b | 0.88 | 221.6 ± 2.7 | 0.54 ± 0.05 | 138 ± 13 | 2451630.9 ± 5.9 |
| | c | 1.63 | 444.6 ± 8.8 | 0.41 ± 0.08 | 96 ± 7 | 2451620.3 ± 12.0 |

it adjacent to stability. If R is changed by less than 5% the system has no chance of surviving even 1 million years. This map shows that the current fit to the system is not correct. However the elements do not need to change by much (specifically e_c needs to be slightly lower) for the system to have a chance at stability.

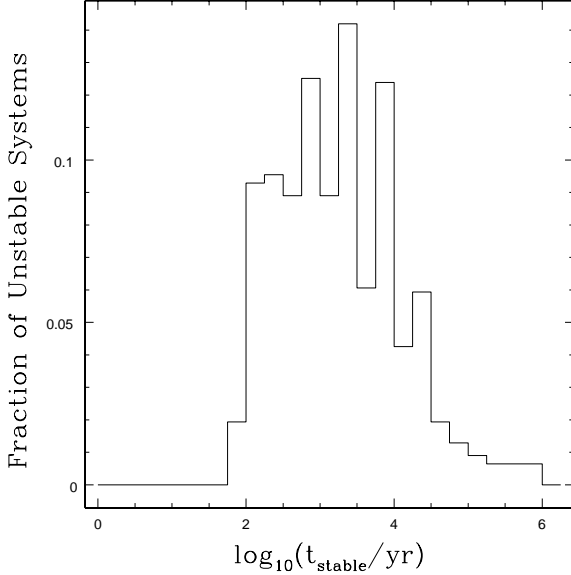


FIG. 1.— The distribution of instability times for unstable configurations of HD82943. Most unstable systems survive for just 10^2 - 10^4 years before perturbations change a semi-major axis by more than a factor of 2.

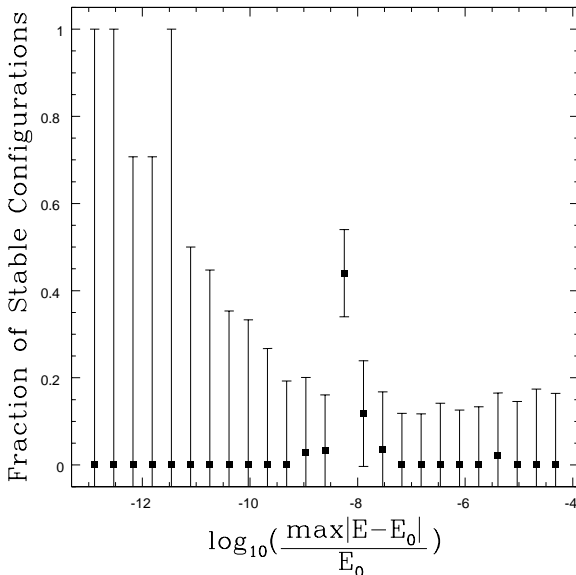


FIG. 2.— Survival rate as a function of energy conservation for HD82943. The lack of a trend implies the results for the system are accurate.

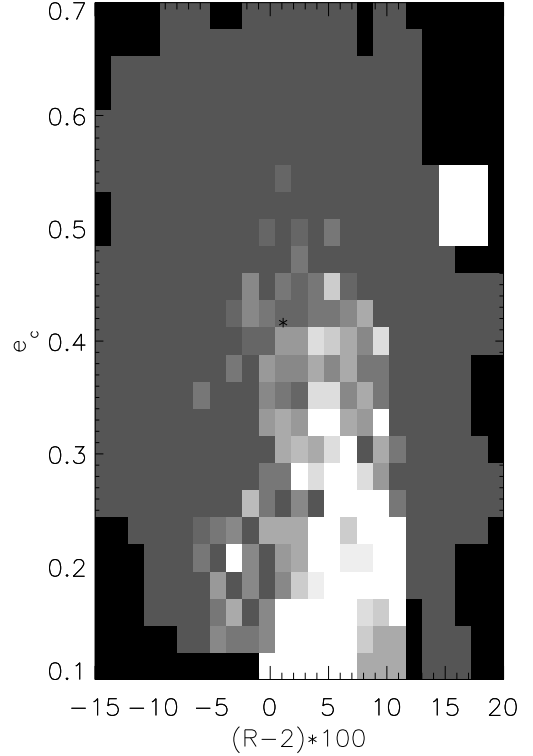


FIG. 3.— The R - e_c stability map for HD82943. The asterisk represents the best fit to the system as of 31 July 2002. The data are most accurate closer to the asterisk. The system shows a clear boundary in phase space between unstable (dark grey) regions and stable (white) regions. Black represents unsampled data. The stable region at $R = 2.15, e_c = 0.52$ is a bin in which 1 out of 1 trials survived.

The system also shows dependence on mean anomaly and longitude of periastron. Because of the symmetry of ellipses we will introduce a new variable, Λ , defined as:

$$\Lambda \equiv \begin{cases} |\varpi_1 - \varpi_2|, & \Lambda < \pi \\ 360 - |\varpi_1 - \varpi_2|, & \Lambda > \pi \end{cases} \quad (5)$$

where the subscripts merely represent 2 different planets, b and c for this system. The order is unimportant, as we are only concerned with the magnitude of this angle. In Fig. 4, the Λ - ΔM stability map is presented. The asterisk marks the best fit to the system. Stability seems to follow a line represented by

$$\Delta M = \frac{4}{3}\Lambda + 120 = \frac{4}{3}(\Lambda + \frac{\pi}{2}). \quad (6)$$

This relation is purely empirical. As is shown in the following sections, this interdependency is unusual for extra-solar planetary systems. Similar plots of ΔM or Λ versus R , show the same R dependence as in Fig. 3. Therefore R is clearly the most important parameter in this system, but these other 3 also play an important role in the system. As more observations of the system are made, HD82943 should fall into the region defined by $1.95 \leq R \leq 2.1$, $e_c < 0.4$, and Eq. 6.

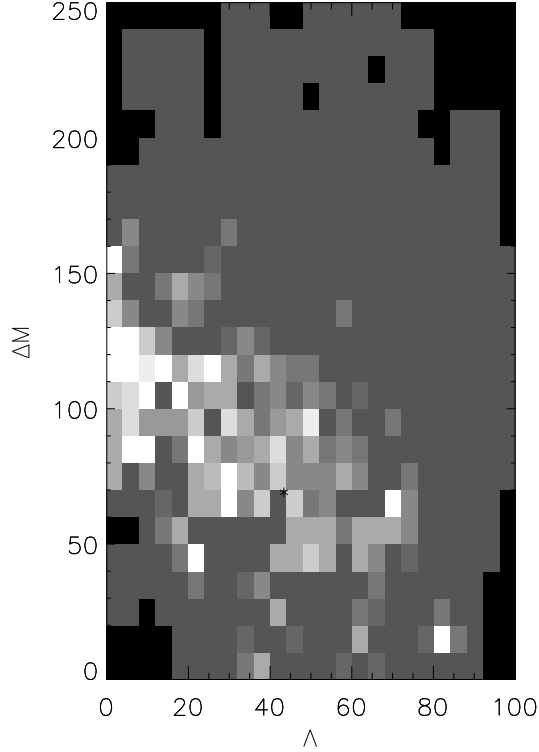


FIG. 4.— The Λ - ΔM stability map for HD82943. The asterisk represents the best fit to the system as of 31 July 2002. The data are most accurate closer to the asterisk. Stability appears to follow the line represented by Eq 6. Note however that the system is also constrained to $\Lambda \leq 75^\circ$ and $\Delta M \geq 30^\circ$. The island at $\Lambda = 80^\circ$, $\Delta M = 20^\circ$ is a bin in which 1 out of 1 trials survived.

HD82943 shows a wide range of dynamics. Some examples of these are shown in Figs. 5-8. The initial conditions of these systems are presented in Table 2. Fig. 5 shows an example of the evolution of a regular system, HD82943-348, which shows no evidence of chaos. Note that instead of $\Lambda(t)$, we present the distribution function of Λ , $P(\Lambda)$, the probability of Λ , vs. Λ . This representation of Λ shows that the motion is like that of a harmonic oscillator; the longitudes of periastron are librating with an amplitude of 60° .

Fig. 6 (HD82943-382) is a stable case which is clearly chaotic. Although the eccentricities remain close to their initial values, the inclinations jump to large values quickly. Note that Λ never exceeds 75° , but its motion is slightly nonharmonic, another indication of chaos.

In Fig. 7 we plot the evolution of a system which ejects planet b. This system experiences close approaches very quickly as is evidenced in the top left panel of Fig. 7. The eccentricities undergo dramatic fluctuations, and the inclinations nearly reach 40° . Although poorly sampled, Λ suggests circulation.

In Fig. 8, the orbital evolution of simulation HD82943-216 is shown. This system perturbed planet c after 280,000 years, and despite the high eccentricities the system obtained (>0.75 for both planets), remained bound for 10^6 years. The inclinations also show large growth. Although initially $\Lambda = 41^\circ$, the system becomes locked at just over 100° . This is misleading as this is the Λ distribution for the full 10^6 years. It is actually the superposition of 2 modes. Initially, until perturbation at 280,000 years, the system circulates with a slight preference toward anti-alignment. However after the perturbation the system

becomes locked at $\Lambda \approx 100^\circ$. Although not shown, after these initial perturbations the system settles down to a configuration in which $a_b \approx 0.344\text{AU}$, $e_b \approx 0.79$ and $a_c \approx 2400\text{AU}$, $e_c \approx 0.99$.

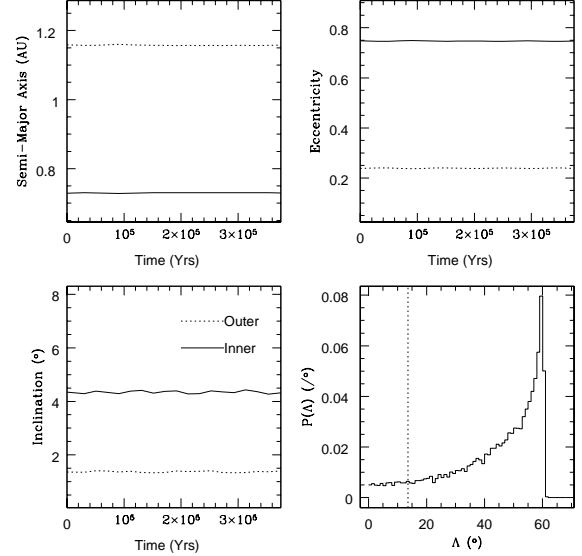


FIG. 5.— Orbital evolution of HD82943-348, a stable, regular configuration. The data here are smoothed over a 20,000 year interval. *Top Left*: The evolution in semi-major axis. The planets show slight variations due to resonant interactions. *Top Right*: The eccentricities oscillate with a 700 year period, with $0.62 \leq e_b \leq 0.85$ and $0.05 \leq e_c \leq 0.45$. This short timescale is not visible in this plot. *Bottom Left*: The inclinations experience oscillations on 2100 year timescale, again too short to be visible in this plot. The ranges of inclination are $1^\circ \leq i_b \leq 7^\circ$ and $0 \leq i_c \leq 3^\circ$. *Bottom Right*: From this distribution function we see the lines of node librate harmonically with an amplitude of 60° . The dashed vertical line represents Λ_0 , the initial value of Λ .

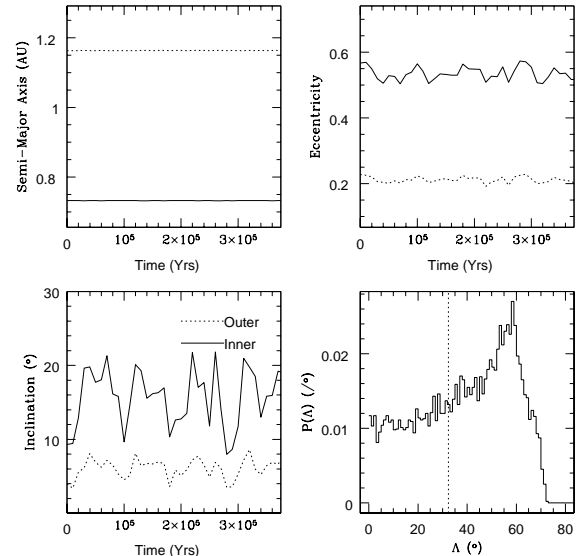


Table 2 - Selected Simulations of HD82943

| Trial | $e_{b,0}$ | $e_{c,0}$ | R_0 | Λ_0 ($^\circ$) | ϵ | Comments ^a |
|-------|-----------|-----------|--------|--------------------------|-----------------------|-----------------------|
| 216 | 0.563 | 0.345 | 2.0108 | 42.2 | 2.6×10^{-7} | C,P(c,299.9) |
| 348 | 0.617 | 0.419 | 1.9656 | 13.6 | 1.5×10^{-8} | R |
| 382 | 0.516 | 0.322 | 2.0303 | 32.4 | 9.2×10^{-9} | C |
| 698 | 0.481 | 0.440 | 2.0948 | 68.4 | 1.3×10^{-10} | C,P(b,7.5),E(b,10.5) |

^a R=Regular, C=Chaotic, P=Perturbed(Planet, Time(10^3 yr)), E=Ejected(Planet, Time(10^3 yr))

FIG. 6.— Orbital evolution of HD82943-382, a stable, chaotic configuration of HD82943. The data are averaged on a 10,000 year interval. *Top Left*: The evolution in Semi-Major Axis. The planets clearly never experience a close encounter. *Top Right*: The eccentricities experience low amplitude ($\approx 13\%$) chaotic oscillations. *Bottom Left*: The inclinations initially jump to large values and experience large amplitude ($\approx 70\%$) fluctuations. *Bottom Right*: The Λ distribution function suggests that Λ is generally librating, but that there are chaotic fluctuations superimposed on this motion. The dashed vertical line is the value of Λ_0 .

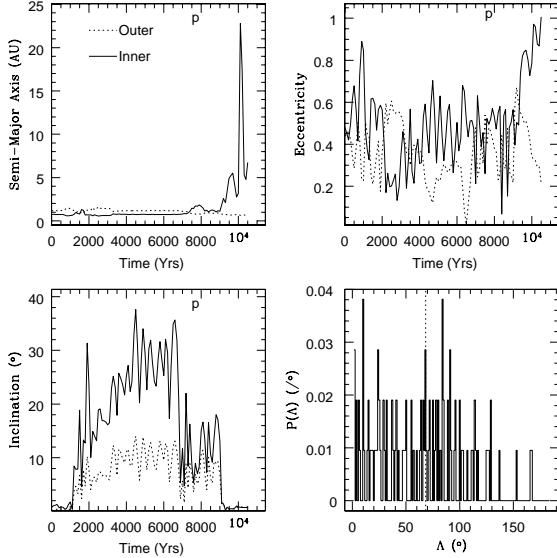


FIG. 7.— Orbital evolution of HD82943-698, the perturbation and ejection of HD82943b. The orbital parameters are sampled every 100 years. *Top Left*: The planets experience close encounters immediately as changes in semi-major axis are visible within 500 years. *Top Right*: The eccentricities experience large amplitude fluctuations, culminating in the ejection of planet b just after 10,000 years. *Bottom Left*: The inclinations vary slightly until a close encounter at 1100 years which sends both inclinations up substantially. The planets remain in this state until just prior to ejection, when they return to coplanarity. *Bottom Right*: The Λ distribution function suggests that Λ remains below 100° , but may occasionally circulate.

We ran 10 simulations for 10^8 years. The initial conditions and results of these simulations are presented in Table 3. The eccentricity evolution of 4 simulations is shown in Fig. 9. These simulations, which ran for 100 million years, show some configurations are regular (top left), some are chaotic (top right, bottom left), and that instability can arise at any timescale (bottom right). These long term simulations show that regions exist in phase space in which this system can survive for billions of years.

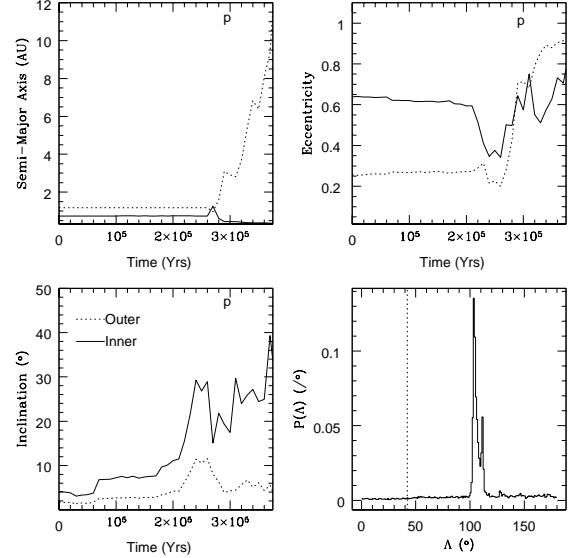


FIG. 8.— Orbital evolution of HD82943-216, the perturbation of HD82943c. The parameters are averaged on 10,000 year intervals. *Top Left*: The planets' semi-major axes are stable and show no signs of close encounters until 260,000 years. At this point planet c actually crosses b's orbit. This initial encounter leads to more encounters as a_c reaches 3AU by 280,000 years, tripping the criterion for instability. *Top Right*: The eccentricities experience secular change until 210,000 years. The system then moves into a lower eccentricity state. The eccentricity then grows to large values and remain at their final values for another 700,000 years. *Bottom Left*: As with eccentricity the inclinations show slow secular change until 210,000 years. The inclinations then leap up to 30° in the case of planet b. *Bottom Right*: The Λ distribution function is the sum of 2 motions: the pre-perturbation motion is circulation, the post-perturbation motion is fixed close to 110° . The dashed line represent Λ_0 .

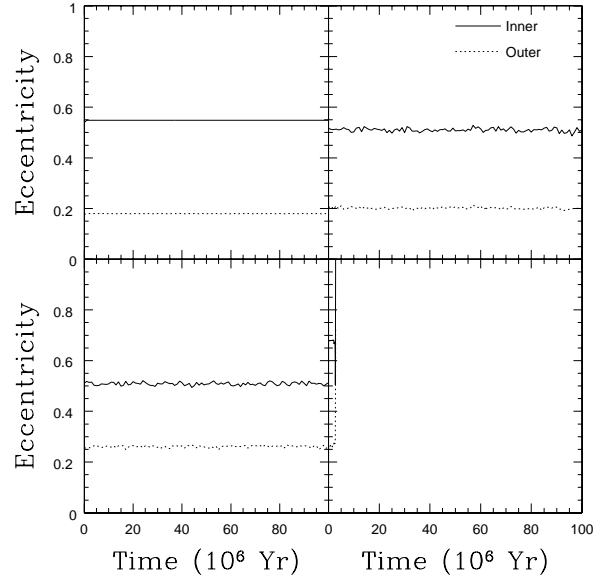


FIG. 9.— Long term simulations of the HD82943 system. These data are averages over 50,000 year intervals. *Top Left*: Evolution of HD82943-035. An example in which the system is regular. *Top Right*: Evolution of HD82943-021, an example of chaotic evolution. *Bottom Right*: Evolution of HD82943-000, another example of chaotic motion. *Bottom Left*: Evolution of HD82943-032. A chaotic system which ejects planet b after 2.4 million years ($7\tau_{HD82943}$).

Table 3 - Results of Long Term (10^8 yr) Simulations of HD82943

| Trial | $e_{b,0}$ | $e_{c,0}$ | R_0 | Λ_0 ($^\circ$) | ϵ | Result ^a |
|-------|-----------|-----------|--------|--------------------------|----------------------|-------------------------------|
| 000 | 0.561 | 0.395 | 2.0269 | 26.5 | 5.2×10^{-8} | C |
| 021 | 0.571 | 0.333 | 2.0615 | 39.0 | 1.0×10^{-8} | C |
| 032 | 0.414 | 0.556 | 2.0556 | 33.3 | 4.95 | $\epsilon(2.4), E(b, 2.4)$ |
| 035 | 0.511 | 0.236 | 2.0322 | 6.7 | 6.8×10^{-9} | R |
| 036 | 0.534 | 0.197 | 2.0080 | 29.5 | 6.1×10^{-9} | R |
| 040 | 0.600 | 0.393 | 2.0766 | 52.8 | 0.22 | $\epsilon(1.005), E(c, 1.14)$ |
| 043 | 0.542 | 0.386 | 2.0223 | 24.8 | 2.4×10^{-8} | C |
| 057 | 0.549 | 0.348 | 2.0382 | 27.0 | 1.1×10^{-8} | C |
| 073 | 0.468 | 0.265 | 2.0626 | 56.8 | 6.3×10^{-8} | R |

^a R=Regular, C=Chaotic, ϵ =Energy conservation failed (Time (10^6 yr)), E=Ejection(Planet, Time (10^6 yr))

Several papers have suggested that secular resonance locking maintains stability in ESPS with large eccentricities (Rivera & Lissauer 2000, Rivera & Lissauer 2001a, Chiang, Tabachnik, & Tremaine 2001). Specifically they suggest that the orientation of the planets' ellipses should be aligned ($\Lambda \approx 0$). By examining Λ in stable, regular long term simulations we can determine if the longitudes of periastron remain locked. The probability distribution of Λ for these same four long term simulations is presented in Fig. 10. Λ is sampled once every 100 years. The top left plot of Fig. 10 is similar to that of an harmonic oscillator; this configuration is librating about $\Lambda=0$ with an amplitude of 40° . The other plots are systems which are not librating, but instead show more random motion. From this figure we see that regular motion is correlated with libration about alignment, but chaotic and unstable generally shows chaotic Λ behavior.

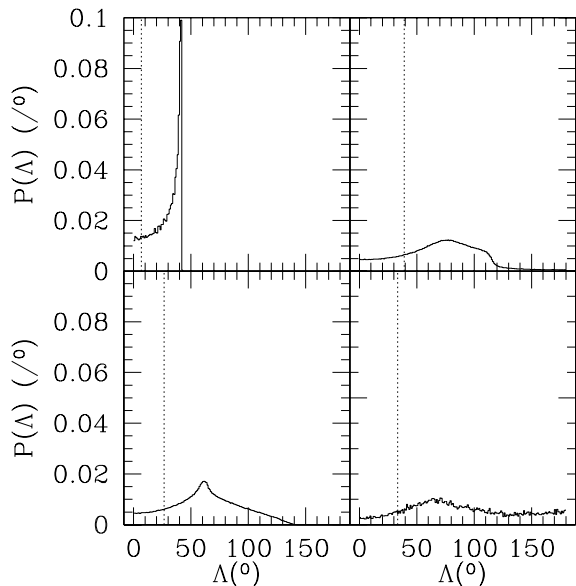


FIG. 10.— The distribution function of Λ (sampled every 100 years) for four stable cases of HD82943. These four systems are the same as in Fig. 9. The top left plots a system librating about $\Lambda=0$. The other plots show that chaotic motion is usually associated with a circulating Λ .

3.2. GJ876

Two planets orbit the $0.32 \pm 0.05 M_\odot$ (Marcy *et al.* 2001a) M4 star GJ876, also known as Gliese 876. This system is very similar to HD82943, the major difference being that the planets lie closer to their primary. The semi-major axes of these two planets are 0.13 and 0.21 AU. Note that in this system planet c is the inner and less massive planet. A substantial amount of work has already been done on this system. Notably, in the discovery paper (Marcy *et al.* 2001) that stable configurations exist in the system. Rivera & Lissauer (2001b) show that Keplerian fitting for this system is not precise enough to accurately determine the orbits. They suggest, through N-body fitting, that GJ876 must actually lie in perfect resonance, and that the orbital elements provided in the discovery paper (which are used here) suffer from a systematic error. Because P_1 is so short for this system (60 days) the evolution of the orbital elements has been observed, and corroborated this theory. This section therefore serves as a check to this hypothesis.

We ran GJ876 for 10^6 years, but τ_{GJ876} corresponds to only 47,000 years. On 47,000 year timescales, only $5.6\% \pm 2.8\%$

of parameter space is stable. On 10^6 year timescales, 2.4% of configurations survived, but only 1.7% were still unperturbed, and 5% failed to conserve energy. In unstable cases planet c, the inner and less massive, was ejected/perturbed nearly 96% of the time. Fig. 11 shows the instability rate. GJ876 shows the same trend as HD82943; most unstable configurations break up in just a few hundred dynamical times. Again the asymptotic nature of this plot implies most unstable configurations have been identified. This system shows the same sort of trend in ϵ as HD82943, which proves that our results are correct.

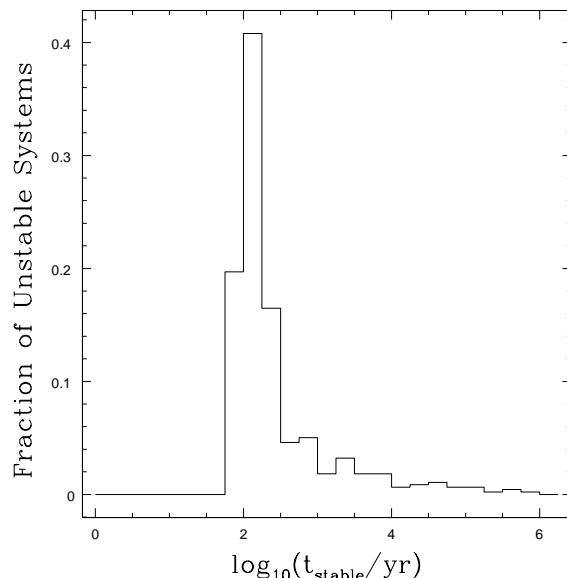


FIG. 11.— The ejection rate for GJ876. In this system unstable configurations are usually ejected within 100 years. The rate asymptotically falls to zero by 10^5 years.

Unlike HD82943, there are no obvious zones of stability. We only see isolated islands in the $R - e_b$ stability map presented in Fig. 12. We choose these parameters for our stability map as they were the strongest indicators of stability in HD82943, and because of the suggestion that the system actually lie in perfect resonance. Close to $R = 2.00$ we sampled two simulations near $R = 2.02$ and $e_b = 0.7$. Both these were stable. However with such poor statistics, and at such a large (relative) distance from perfect resonance, we cannot comment on the likelihood that the system would be more stable in perfect resonance. We can, however, point out that there are isolated configurations which may hold stable orbits, and prolonged observations of this system should demonstrate whether it is indeed in perfect resonance. However this lack of a large stable region strengthens the hypothesis that this system lies in perfect resonance.

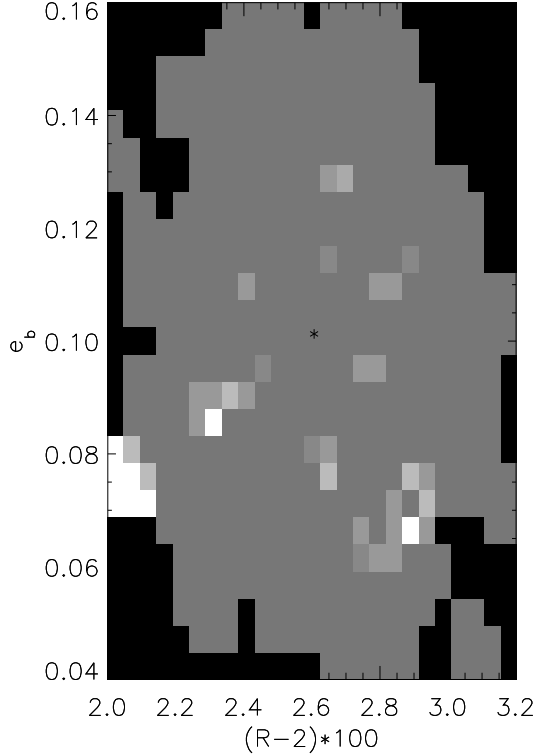


FIG. 12.— The R - e_b stability map for GJ876. The asterisk marks the best fit to the system as of 7 Aug 2002, and the values for stability are more accurate closer to the asterisk. In this system, as in HD82943, the two relevant orbital elements are e_1 and R . There are no contiguous regions of stability, only small isolated pockets which may hold stable zones.

This system does, however, lie very close to $\Lambda=0$. However this proximity to alignment has no bearing on the stability of the system, in fact, it may actually diminish its chances of stability. In Fig. 13 the probability of stability as a function of initial Λ is shown. Although the values for large Λ are poorly sampled, four data points at 100% stability does suggest larger values of Λ may be more stable.

Similar dynamics are present in GJ876 as in HD82943. In Figs. 14-17, we show 4 examples of stable and unstable configurations. The initial conditions for these sample simulations are listed in Table 4. In Fig. 14 the orbital evolution of simulation GJ876-904 is shown. This system is one of very few (<10) simulations which show approximately regular motion. The semi-major axes show resonant perturbations, and Λ shows a motion typical of chaos; it appears to be the superposition of libration and circulation.

In Fig. 15 the evolution of a stable, yet chaotic, configuration is plotted. Although this system was stable for 47,000 years, planet b was perturbed after 220,000 years. This system however remained bound for 10^6 years. The large eccentricity oscillations continue on to 10^6 years, and planet c tends to remain in a retrograde orbit. After 10^6 years $a_c = 0.0515\text{AU}$, $0.06 \leq e_c \leq 0.85$, $i_c \approx 120^\circ$, $a_b \approx 0.87\text{AU}$, $e_b \approx 0.77$, and $i_b \leq 5^\circ$. The period of e_c oscillations remains at 3300 years. The Λ evolution further belies the chaos in this system, as it tends toward anti-alignment, but also circulates. As before this distribution is over 10^6 years, but as the system remains in approximately the same state from 25,000 years to 10^6 years, this plot is a fair representation of the motion during the first τ_{GJ876} .

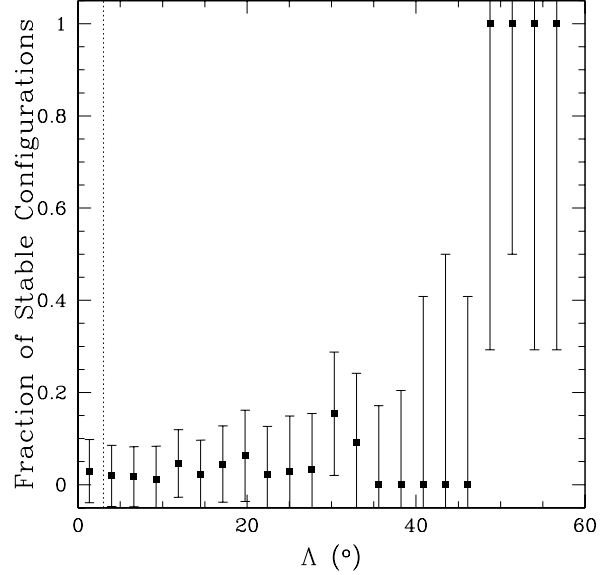


FIG. 13.— The dependence of stability on initial Λ . The data above 50° are poorly sampled, but with such a large difference between their values and the mean of 5.7%, they do suggest that stability may be improved at $\Lambda \gtrsim 50^\circ$.

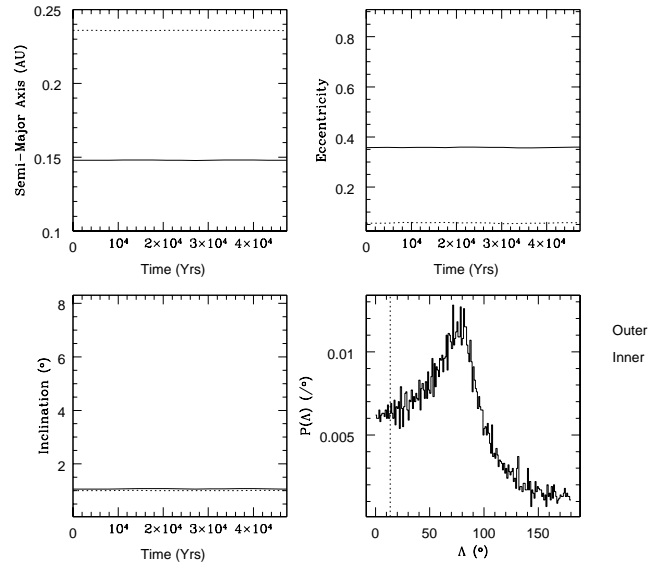


FIG. 14.— Orbital evolution of GJ876-904, the stable, regular motion of GJ876. The data are smoothed on 3000 year intervals, which eliminates all short period behavior. *Top Left*: The low order resonance and large eccentricities induce low amplitude oscillations in the semi-major axes of the planets with a period of 2 years. This short frequency is not visible in this plot due to the smoothing interval. *Top Right*: The evolution of eccentricity for this configuration is that of two eigenmodes, also on a period of 2 years. *Bottom Left*: The inclinations vary slightly with a frequency of 250 years. *Bottom Right*: The Λ distribution function suggests that Λ sometimes librates with an amplitude of $\approx 80^\circ$, and sometimes circulates. The dashed line marks Λ_0 .

Table 4 - Selected Simulations of GJ876

| Trial | $e_{c,0}$ | $e_{b,0}$ | R_0 | Λ_0 ($^{\circ}$) | ϵ | Comments ^a |
|-------|-----------|-----------|--------|----------------------------|----------------------|--------------------------|
| 029 | 0.177 | 0.073 | 2.0241 | 11.6 | 4.6×10^{-5} | C |
| 563 | 0.239 | 0.122 | 2.0247 | 3.65 | 2.2×10^{-8} | C, P(b,5.1), E(b,5.3) |
| 858 | 0.338 | 0.107 | 2.0255 | 13.1 | 6.2×10^{-6} | C, P(c,14.9), E(c,151.9) |
| 904 | 0.351 | 0.072 | 2.0303 | 51.0 | 2.7×10^{-9} | R? |

^a R=Regular, C=Chaotic, P=Perturbed(Planet, Time (10^3 yr)), E=Ejected(Planet, Time (10^3 yr))

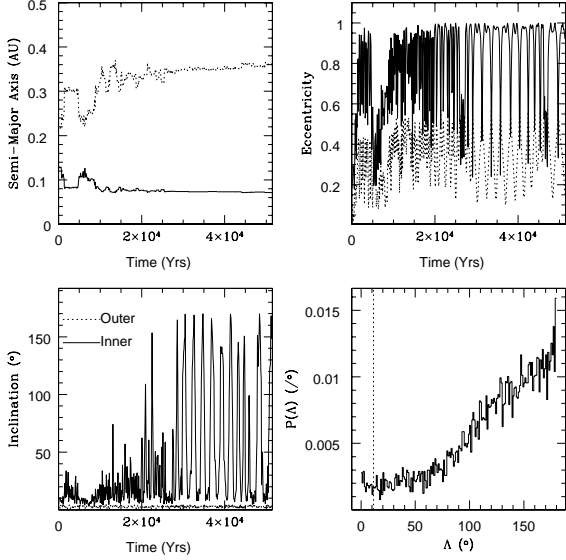


FIG. 15.— Orbital evolution of GJ876-029, a chaotic stable configuration of GJ876. *Top Left*: Although the semi-major axes vary, they don't change by a factor of 2 until $220,000 \text{ years} = 4.7\tau_{\text{GJ876}}$. *Top Right*: The remarkable eccentricity evolution of this system. These oscillations persist for 10^6 years. *Bottom Left*: The inclination of planet b varies a small amount, generally staying below 5° . Planet c however experiences wild fluctuations, however it does eventually settle to 120° . *Bottom Right*: This curious Λ distribution function suggests that Λ prefers anti-alignment. This implies that a protection mechanism is keeping the system from breaking apart despite the extremely large values of e_b .

In Fig. 16, the evolution of GJ876-563 is shown. This configuration ejects planet c in just over 5000 years. The system shows evidence for close approaches right from the beginning as the semi-major axes show small amplitude, chaotic fluctuations. The inclinations and eccentricities also experience a large degree of chaos. Although initially Λ is very close to 0, it circulates for the duration of the simulation.

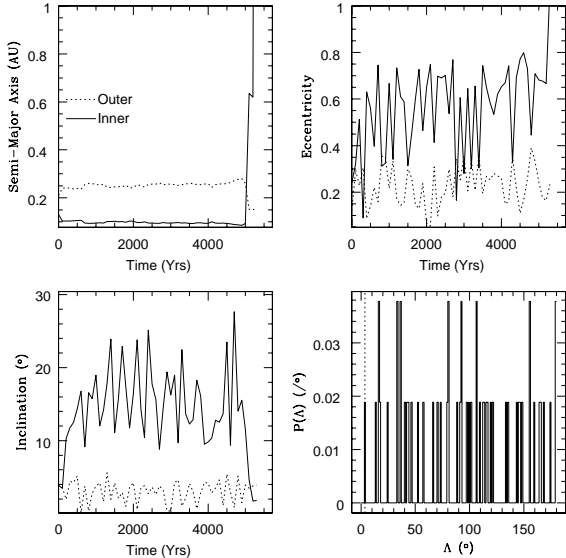


FIG. 16.— Orbital evolution of GJ876-563, the ejection of GJ876c. *Top Left*: The semi-major axes undergo small fluctuations until a violent encounter ejects the inner planet after 5000 years. *Top Right*: The eccentricities experience large amplitude fluctuations, until e_c eventually reaches unity. *Bottom Left*: The inclination of planet b initially jumps and remains at over 30° , but then returns to coplanarity just before ejection. This type of motion was also seen in Fig. 8. *Bottom Right*: As with the majority of chaotic configurations, Λ circulates. Although poorly sampled, Λ appears to have no preferred value.

In Fig. 17 the evolution of a system which perturbs the outer planet in just 9000 years is shown. The system ejects planet b in 152,000 years. Before reaching τ_{GJ876} this system experiences some remarkable evolution in a , e , and i . Note, too, that Λ very quickly moved to an anti-aligned configuration.

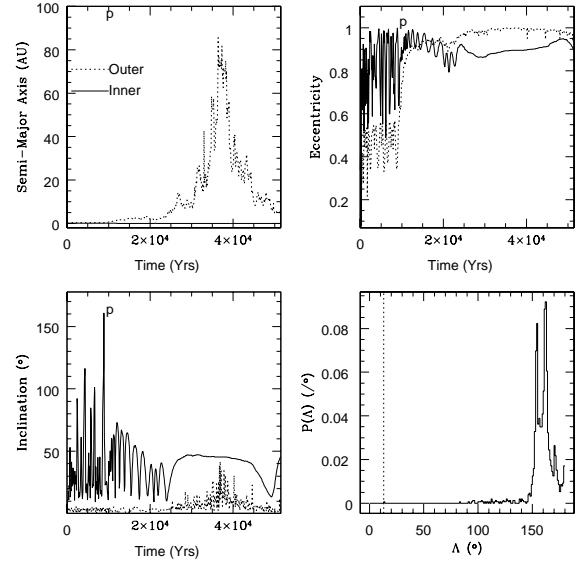


FIG. 17.— Orbital evolution of GJ876-858, the perturbation of GJ876b. Planet b was eventually ejected after 152,000 years. *Top Left*: The semi-major axes evolve quiescently for 9000 years, until a close approach increases a_b , marked by the p. Although a_b returns to its initial value by τ_{GJ876} , just prior to ejection a_b reached 750AU. *Top Right*: The eccentricities immediately jump to very large values. e_c varies wildly between 0.6 and 0.99. After b is kicked out to large a , the oscillations become much smaller. For nearly 10,000 years e_b remains above 0.98, but it doesn't reach unity until 152,000 years. *Bottom Left*: As with eccentricity, the inclination of c jumps wildly for 9000 years, even reaching 162° just prior to perturbation. However it is unclear if this large inclination produces the perturbation. *Bottom Right*: As with the e and i , Λ immediately moves from its starting position. However Λ remains very close to anti-alignment for the duration of the simulation.

Long term simulations for this system were integrated for 27.5 million years. A complete summary of the long term simulations for this system is presented in Table 5. Fig. 18 plots the eccentricity evolution of 4 simulations. Some systems appear regular throughout (top left). Some configurations are chaotic for the duration of the simulation (top right, bottom left), and others may eject a planet after an arbitrarily long period of time (bottom right).

Table 5 - Results of Long Term (27.5×10^6 yr) Simulations of GJ876

| Trial | $e_{c,0}$ | $e_{b,0}$ | R_0 | Λ_0 ($^\circ$) | ϵ | Result ^a |
|-------|-----------|-----------|---------|--------------------------|----------------------|------------------------------|
| 290 | 0.0884 | 0.248 | 2.02353 | 45.3 | 2.4×10^{-9} | C |
| 300 | 0.108 | 0.161 | 2.02641 | 15.2 | 0.5 | $\epsilon(4.06)$, E(b,4.08) |
| 362 | 0.124 | 0.366 | 2.02624 | 29.3 | 2.6×10^{-8} | R |
| 404 | 0.121 | 0.246 | 2.02548 | 46.43 | 0.6 | $\epsilon(17.6)$, C |
| 609 | 0.0875 | 0.241 | 2.02342 | 53.5 | 2.5×10^{-9} | R |
| 655 | 0.110 | 0.256 | 2.02601 | 13.9 | 0.19 | $\epsilon(11.2)$, P(b,24.0) |
| 661 | 0.105 | 0.208 | 2.02778 | 33.1 | 0.18 | $\epsilon(2.4)$, E(c,2.4) |
| 739 | 0.107 | 0.273 | 2.02726 | 31.2 | 0.02 | $\epsilon(1.4)$, E(b,1.4) |
| 895 | 0.0816 | 0.228 | 2.02242 | 19.4 | 2.3×10^{-8} | C |
| 948 | 0.0628 | 0.204 | 2.02803 | 4.80 | 4.1×10^{-4} | $\epsilon(0.25)$, C |

^a R=Regular, C=Chaotic, ϵ =Energy conservation failed (Time 10^6 yr)), P=Perturbed (Planet, Time (10^6 yr)), E=Ejected (Planet, (10^6 yr))

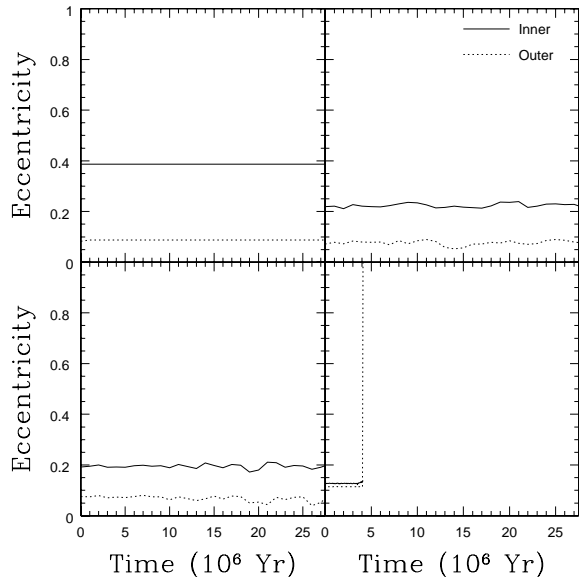


FIG. 18.— Eccentricity of 4 long term simulations of GJ876. *Top Left*: Evolution of GJ876-362, a regular configuration. *Top Right*: Evolution of GJ876-290, a chaotic, yet stable configuration. *Bottom Left*: Evolution of GJ876-895, a chaotic, stable configuration. *Bottom Right*: Evolution of GJ876-300 which ejects planet b after 4 million years.

Fig. 19 shows the distribution function of Λ for the same four systems. The regular system (top left) shows a configuration which usually librates with an amplitude of 80° , but with occasional circulation. The two chaotic examples (top right, bottom left) have flat distribution functions. Not surprisingly the unstable trial shows a very peculiar distribution function. As in HD82943 we see that regular systems tend to librate, and chaotic configurations circulate.

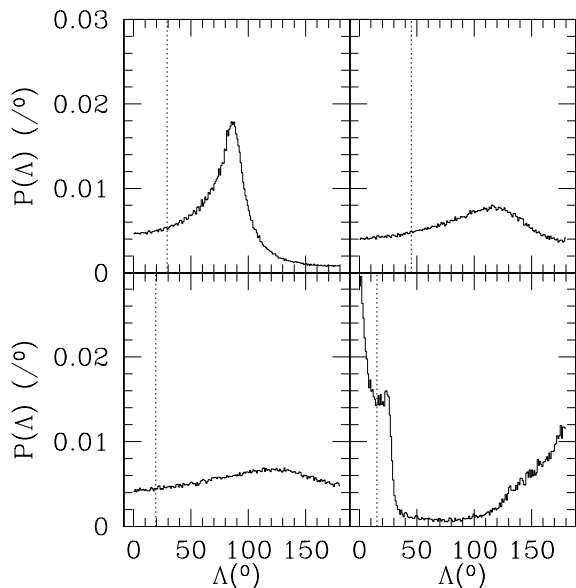


FIG. 19.— The Λ evolution of the same four simulations in Fig. 19. Chaotic systems (top right, bottom left) show no signs of libration, while regular systems (top left) are librating, but with occasional circulation. The unstable example (bottom right) shows a very strange distribution, which only demonstrates the chaos of this system.

³http://ssd.jpl.nasa.gov/elem_planets.html

Although the evidence is compelling that GJ876 does in fact lie in perfect resonance, our work demonstrates that stable, regular systems do exist close to the observed Keplerian fit. More observations of this system will demonstrate if the system is in perfect resonance. This work clearly demonstrates that stable regions do exist for a system like GJ876 just beyond perfect resonance. Should this system lie in perfect resonance, then this work shows that unstable regions lie very close to its configuration.

New astrometric data has confirmed the mass of the outer planet in this system (Benedict *et al.* 2002). This therefore provides the only system with a known mass. The plane of b's orbit is inclined by 6° to the line of sight. Benedict *et al.* confirm the mass and semi-major axis of this planet to be statistically identical to those presented in Table 1. However for this paper, the lack of data for planet c precludes any new insights into the dynamics of the system. At best, if the system is approximately coplanar, then the variations used here are indeed representative of the true system, and our results are more robust.

4. INTERACTING SYSTEMS

Four known systems meet the interacting system criterion: ν And (Butler *et al.* 2000), 47UMa (Fischer *et al.* 2002), the SS³ and HD12661 (Fischer *et al.* 2003). In this paper we will limit ourselves to the first three. The number, placement, and size of the planets in each system are quite different, but all have at least two planets that lie in between the 2:1 and 10:1 resonances. ν And was the first known ESPS, and was the subject of Paper I. The experiment in Paper I is the procedure for this paper, and the simulations have been performed again. 47UMa was announced in 2001, and, at first glance, appears more like the SS than ν And. Performing this experiment on the SS is problematic. The errors in the orbital elements of the SS are drastically smaller than for the ESPS, therefore fitting the SS into the procedure requires inflating the SS orbital element errors to values comparable to those of the ESPS. Essentially we are asking what would we observe if we took radial velocity measurements of our sun. We will compare the ESPS to both the gas giant system (§4.3) and the Jupiter-Saturn system (§4.4). These three coupled systems' orbital elements are summarized in Table 6. Interacting systems show broad regions of stability which are correlated with eccentricity.

4.1. ν Andromedae

The ν And system is a combination of a separated system and an interacting system. Three planets orbit the $1.02 \pm 0.03 M_\odot$ (Gonzalez & Laws 2000) F8 star ν And. The inner planet, b orbits at 0.04AU. The other planets, c and d, orbit at larger distances (0.8AU and 2.5AU respectively), but are significantly more eccentric. The outer planet is the most massive, therefore $\tau_{\nu And}$ corresponds to 10^6 years.

The ν And system was the subject of Paper I, and has been the focus of intense research since its discovery. The apparent alignment of the apses of planets c and d has sparked the most interest with several groups claiming that the system must be secularly locked, or at least librate about $\Lambda=0$ (Rivera & Lissauer 2000; Rivera & Lissauer 2001b; Chiang, Tabachnik, & Tremaine 2002), while others suggest this alignment may be a chance occurrence (Paper I; Stepinski, Malhotra, & Black 2000). However, these groups and others (Laughlin & Adams 1999) all agree that this system, as presented, can be stable for

Table 6 - Initial Conditions for Interacting Systems

| System | Planet | Mass(M_J) | Period(d) | Eccentricity | Long. of Peri.(Deg) | Time of Peri. (JD) |
|--------------|---------|---------------|----------------------|-------------------|---------------------|-----------------------|
| SS | Jupiter | 1.000 | 4331.6 ± 43.3 | 0.0484 ± 0.1 | 14.8 ± 90.0 | 2449896.3 ± 25.0 |
| | Saturn | 0.297 | 10759.7 ± 107.8 | 0.0542 ± 0.1 | 92.4 ± 90.0 | 2450411.1 ± 25.0 |
| | Uranus | 0.0459 | 30704.9 ± 307.0 | 0.0472 ± 0.1 | 171.0 ± 90.0 | 2447230.0 ± 25.0 |
| | Neptune | 0.0541 | 60197.2 ± 602.0 | 0.0086 ± 0.1 | 45.0 ± 90.0 | 2442071.3 ± 25.0 |
| <i>v</i> And | b | 0.69 | 4.61706 ± 0.0003 | 0.015 ± 0.015 | 32.0 ± 243.0 | 2459991.588 ± 3.1 |
| | c | 1.96 | 241.1 ± 1.1 | 0.25 ± 0.11 | 251.0 ± 33.0 | 2450160.1 ± 20.8 |
| | d | 3.98 | 1309.0 ± 30.0 | 0.34 ± 0.11 | 255.0 ± 17.0 | 2450044.0 ± 40.5 |
| 47UMa | b | 2.54 | 1089.0 ± 3.0 | 0.06 ± 0.014 | 172.0 ± 15.0 | 2453622.0 ± 34.0 |
| | c | 0.76 | 2594.0 ± 90.0 | 0.1 ± 0.1 | 127.0 ± 56.0 | 2451363.5 ± 493.0 |

at least 10^8 years.

On a 10^6 year timescale, $86.1\% \pm 3.3\%$ of simulations survived, and 0.4% failed to conserve energy. This value is less than 1σ from the value published in Paper I, $84.0\% \pm 3.4\%$. Fig. 20 shows the perturbation rate as a function of time. Once again we see that most unstable configurations eject a planet immediately, and the rate falls to 4% by 10^6 years. The fact that ejections occur right up to 10^6 years implies that we have not detected all unstable situations, and that the stability map for this system contains more unstable configurations, and hence the plateau is smaller and/or the edge is steeper after 10^9 years.

There is one notable difference between the results of Paper I, and those reported here: the frequency of ejections of each planet is different. In Paper I planet b was ejected 10% of the time, c, 60%, and d, 30%. The SWIFT runs ejected planet b 39% of the time, c, 54%, and d, 7%. Fig. 21 plots the survival probability in this system as a function of energy conservation. Stability peaks at $\epsilon = 10^{-8}$ but quickly drops. Although this plot is qualitatively different from Fig. 2, we again note that this implies the simulations are valid. This plot is typical for the interacting systems, confirming our hypothesis that we need only maintain $\epsilon < 10^{-4}$ for the duration of every simulation.

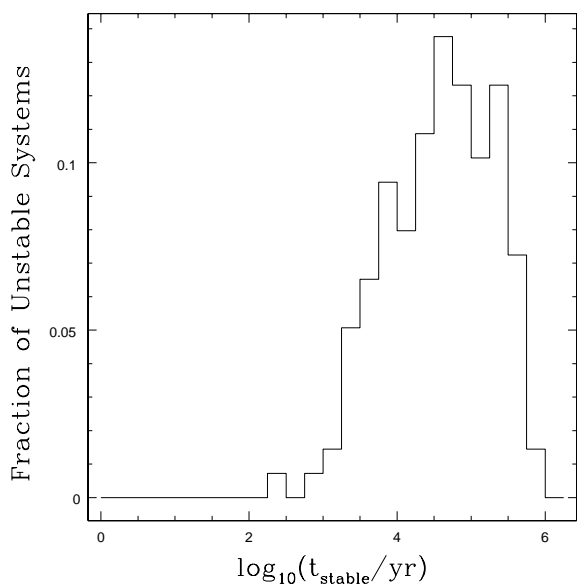


FIG. 20.— The ejection rate of unstable configurations in ν And. Configurations may eject planets right up to 10^6 years. It is therefore unclear how many more configurations might become unstable.

In Paper I, a stability map in e_c and e_d was presented in Table 2. This table showed that e_d and, to a lesser degree e_c determined the stability of the system. In Fig. 22, the ν And stability map is presented. It is nearly an exact match to that in Paper I. However the best fit to the system⁴ has changed since then and the system has moved away from the edge slightly. It is important to note that two different integration schemes produced the same results. From Fig. 22, it is clear that ν And lies near instability. The edge of stability in ν And, however, is fundamentally different than in resonant systems. In this interacting system, a large region of phase space is fully stable, the “plateau”, but there is a sharp boundary in eccentricity space, the “edge”, beyond which the system quickly moves into a fully unstable region, the “abyss”. Although it appears that both morphologies are on the edge of stability, they are different types of

⁴<http://exoplanets.org/upsandb.html>

edges.

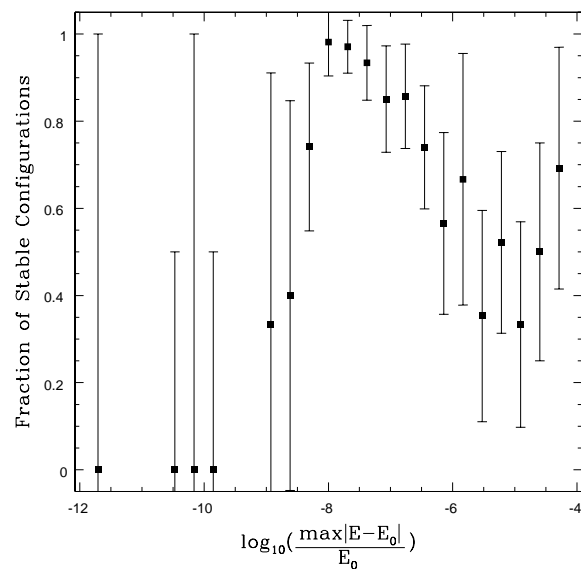


FIG. 21.— Survival probability as a function of energy conservation in ν And. The instability at low ϵ implies the results for ν And are robust.

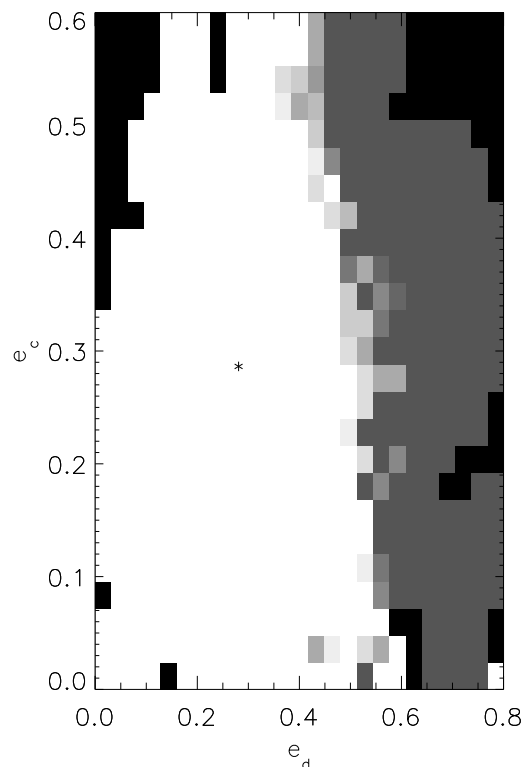


FIG. 22.— Stability map for ν And. Stability in this system depends on e_d and, to a smaller degree, on e_c . As in resonant system stability maps, precision is correlated with distance from the asterisk, which marks the best fit to the system as of 24 Sept 2002. ν And lies near the edge of stability.

As previously mentioned there are some unusual features of this system; the lines of node are nearly aligned, and the system

lies close to the 11:2 mean motion resonance. This is a weak perturbation, but between these 2 massive planets, this may be important. However a quick inspection of plots of stability versus Λ , Fig. 23, and R , Fig. 24, shows that there is no statistically significant affect caused by these to (potential) resonances. We do note that our integration time may not be long enough to detect the importance of the 11:2 resonance.

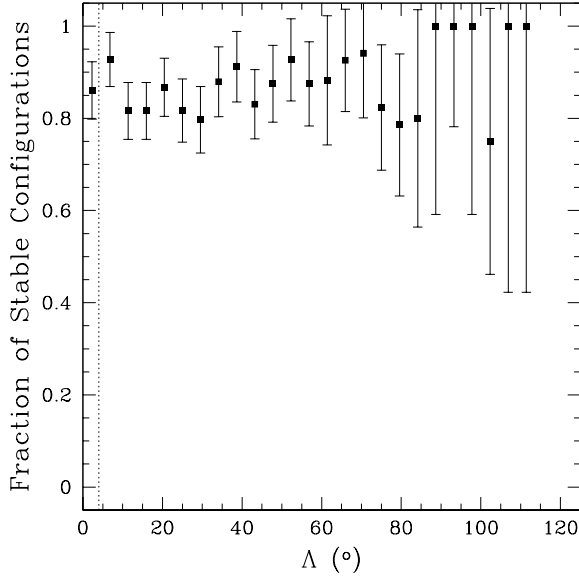


FIG. 23.— Stability as a function of Λ in v And. Although the best fit to the system places it very close to alignment, marked by the dashed vertical line, there is no significant trend with Λ .

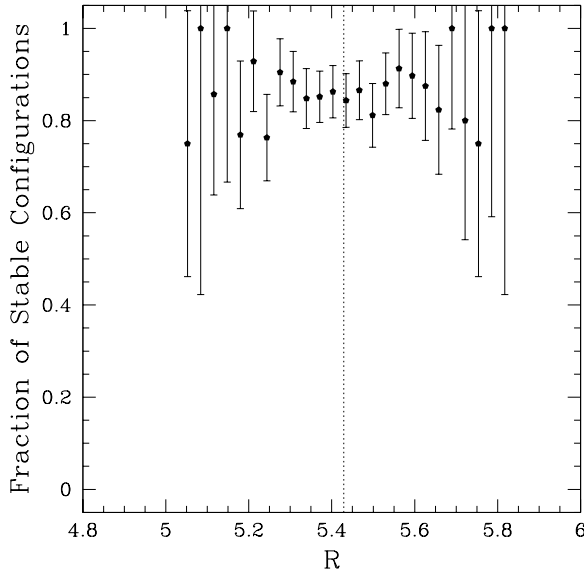


FIG. 24.— Stability as a function of R in v And. There is no evidence that this weak mean motion resonance affects the stability of v And. Although there are fully stable points outside of resonance, all vary by less than 1σ of the mean stability rate of 0.86.

As has been shown in other papers, this system exhibits both regular, and chaotic motion. In Figs. 25-29, we present 5 examples of this system. The initial conditions of these configurations are listed in Table 7. In Fig. 25, the orbital evolution of a regular, stable configuration is plotted. However, this plot

actually demonstrates the breakdown of our model. Planet b's eccentricity oscillates with an amplitude of 0.3 and a period of 120,000 years. Unfortunately, v And b is tidally locked by its parent star with a period of 0.011 years. The timescale for tidal circularization is 8×10^7 yrs (Trilling 2000). We address this potential inconsistency in §7. Λ for this system librates with an amplitude of 50° , an indicator of regular motion.

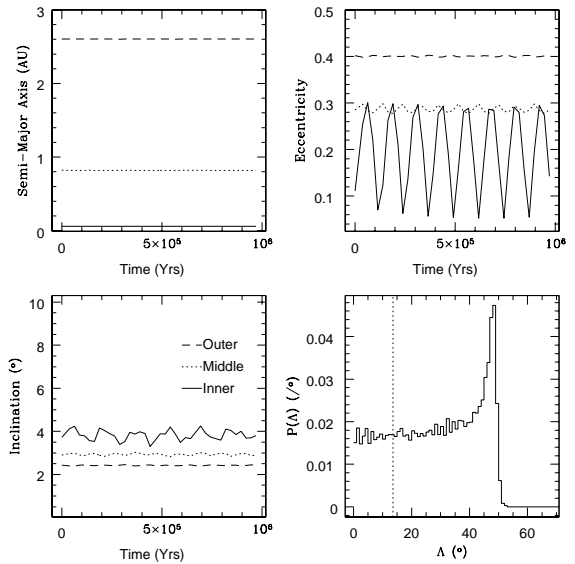


FIG. 25.— The orbital evolution of v And-076, a stable, regular configuration, smoothed on 25,000 year intervals. *Top Left:* The semi-major axes show no evidence of perturbations. *Top Right:* The eccentricities experience simple sinusoidal variations. The period of planet b oscillations is 100,000 years, while c and d oscillate on a 7000 year period. The large amplitude of e_b is most likely unphysical due to tidal locking with the parent star. The apparently irregular behavior of e_b is an artifact of its long cycle. *Bottom Left:* The inclinations are also regular, although planet b's inclination is affected by both planets on its 20,000 year period. Planets c and d oscillate in inclination on a 4000 year period. As in eccentricity, the slightly chaotic appearance of i_b is an artifact of the sampling time convolved with the physical period. *Bottom Right:* The Λ distribution librates with an amplitude of 50° .

In Fig. 26 the evolution of a stable, but chaotic system, v And-236, is presented. In this configuration a_d is mildly perturbed, but the eccentricities and inclinations undergo wild fluctuations. Λ also shows evidence of chaos as it librates and circulates.

Table 7 - Selected Simulations of v And

| Trial | $e_{c,0}$ | $e_{d,0}$ | R_0 | Λ_0 ($^\circ$) | Comments ^a |
|-------|-----------|-----------|-------|--------------------------|-------------------------|
| 000 | 0.276 | 0.486 | 5.583 | 38.3 | C, P(c,218), E(b,218) |
| 014 | 0.177 | 0.470 | 5.509 | 20.2 | C, P(d,219), E(d,219) |
| 020 | 0.299 | 0.532 | 5.207 | 21.7 | C, P(d,10.1), E(c,31.3) |
| 076 | 0.394 | 0.375 | 5.566 | 11.1 | R |
| 236 | 0.168 | 0.428 | 5.386 | 81.0 | C |

^a R=Regular, C=Chaotic, P=Perturbed(Planet, Time(10^3 yr)), E=Ejected(Planet, Time(10^3 yr))

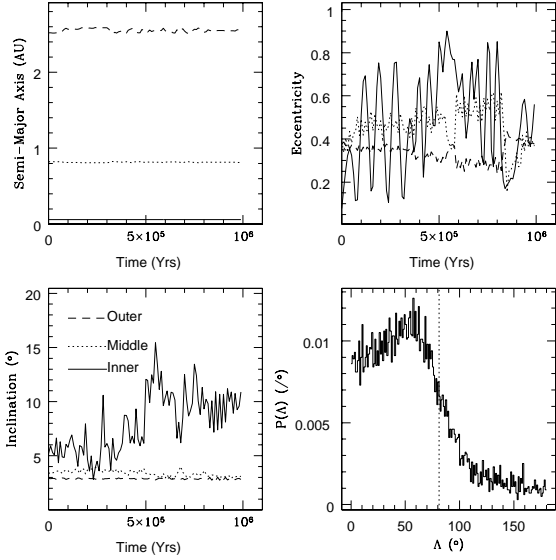


FIG. 26.— The orbital evolution of v And-236, a stable, chaotic configuration. *Top Left*: The semi-major axes show perturbations of planets c and d. *Top Right*: The eccentricities are quite chaotic, especially e_b . However, we see very large eccentricities, and low semi-major axes for planet b. This again suggests that these large values may be unphysical. However, this does not change the fact that this system is chaotic. *Bottom Left*: The inclinations also show a large degree of chaos. As with the eccentricities, it is b which shows the most deviations from regular motion. *Bottom Right*: The Λ distribution suggests that this system librates and circulates. This is the typical behavior of a chaotic system.

v And may eject any planet. However, as demonstrated in Fig. 25, the model breaks down for large e_b . The path to ejection for one such ejection of planet b is shown in Fig. 27. The eccentricities stay generally low (<0.2) for nearly 200,000 years, but prior to ejection e_b grows to 0.99 at times, before finally being ejected.

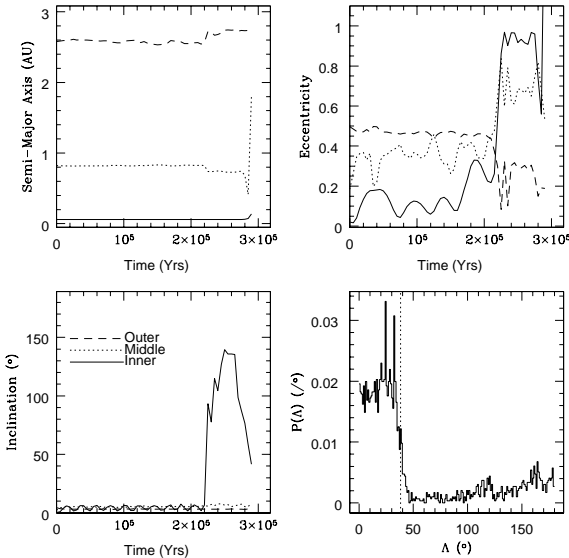


FIG. 27.— The orbital evolution of v And-000, the ejection of v And b. *Top Left*: The system appears to be experiencing perturbations right from the start as a_d evolves chaotically. Eventually a close approach between b and c produces an ejection. *Top Right*: Once again we see that tidal circularization would alter the outcome of this trial. Although it is unclear if circularization would have been enough to prevent the close approach that ejects planet b. *Bottom Left*: In contrast to eccentricity, inclination evolves regularly for 200,000 years, when a close approach sends b into a retrograde orbit, while i_c and i_d continue to evolve sinusoidally. *Bottom Right*: This unusual Λ distribution function reveals further chaos in the system, and, as is seen in other systems, appears to be the sum of a libration mode, and a circulation mode.

In Fig. 28 we show the orbital evolution of a system which perturbs planet d, but ejects planet c. The behavior of the ejecting planet reaching very large semi-major axis distances, and subsequently returning, only to be ejected was also seen in Fig 17. Note, too, that the peak in e_b corresponds with i_b .

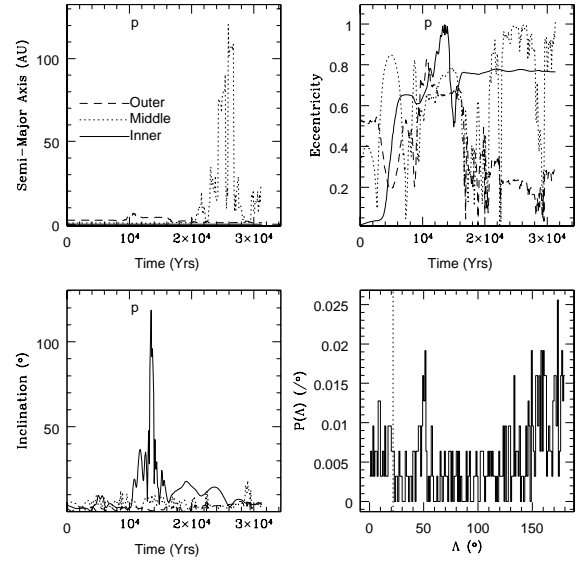


FIG. 28.— The orbital evolution of v And-020, the ejection of v And c. *Top Left*: The semi-major axes evolve quiescently for 10,000 years before perturbing planet d, marked by the p . 10,000 years later planet c is perturbed to over 120AU. The planet then returns to low a , but is quickly ejected after another encounter with planet d. *Top Right*: This configuration experiences wild oscillations from the very beginning. *Bottom Left*: The inclinations also suffer large, chaotic fluctuations. Shortly after planet d is perturbed, planet b experiences a short period of retrograde motion. *Bottom Right*: Although poorly sampled, this graph clearly shows that Λ evolves chaotically.

Finally we show the ejection of planet d, the most massive planet in the system in Fig 29. This system evolves quasi-regularly for 200,000 years before suddenly ejecting planet d. The only hints of chaos are in the evolution of e_c and e_d , although there are some slight asymmetries in the sinusoidal evolution of e_b . Λ is generally librating, although in the final 20,000 years it does circulate as the system destabilizes.

Long term simulations run for 100 million years. Fig. 30 is the eccentricity evolution of 4 simulations. In one case (bottom right panel of Fig. 30) the inner planet is ejected after 55 million years. The top left panel shows a system undergoing chaotic evolution. The other two panels show regular motion.

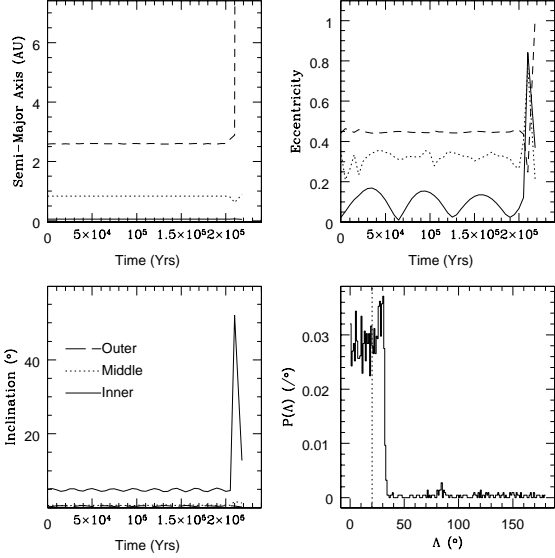


FIG. 29.— The orbital evolution of *v* And-014, the ejection of *v* And d. *Top Left*: The semi-major axes evolve without perturbation for 200,000 years before planet d is suddenly flung from the system. *Top Right*: This configuration experiences low amplitude chaos in its eccentricity until it suddenly experiences a close approach at 200,000 years. *Bottom Left*: The inclinations, however, evolve regularly until a close approach sends b into a 45° orbit. A second close approach kicks it back down, but d is ejected before it returns to the orbital plane. *Bottom Right*: This plot shows the typical behavior of Λ ; it librates while motion is regular, but circulates after close approaches destabilize the system. Here, the Λ distribution represents 200,000 years of libration and 25,000 years of circulation.

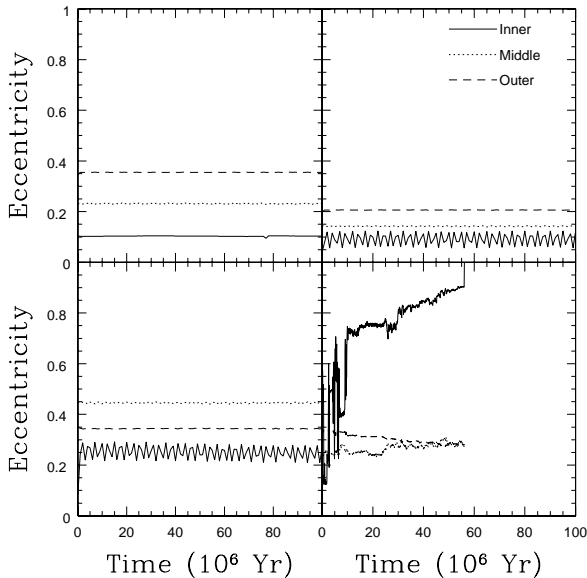


FIG. 30.— The long-term eccentricity evolution of 4 simulations of *v* And. *Top Left*: Eccentricity evolution of *v* And-006. This is an example of regular evolution. *Top Right*: Eccentricity evolution of *v* And-054. This is a chaotic configuration. The chaos has been mostly smoothed over, though, as the data represent 10,000 year averages. *Bottom Left*: Eccentricity evolution of simulation *v* And-288. Another chaotic configuration. *Bottom Right*: Eccentricity evolution of *v* And-192. A chaotic system which ejects the inner planet after 55 million years. This evolution is suspect as the effects of tidal circularization undoubtedly play a role in the evolution of e_b .

Fig. 31 shows the Λ distribution of these configurations. Secular resonance locking does not occur in the *v* And system; the ellipses tend to be anti-aligned. This is the same result as in Paper I. However there do appear to be several different modes of stability for the apses in this system. The panels in Fig. 31 correspond to those in Fig. 30, therefore the top left is the regular case. The chaotic systems (top right, bottom left) show the Λ distribution signature of chaos, as does the example which ejects planet b (bottom right). In Table 8 we present a summary of all long term simulations for *v* And.

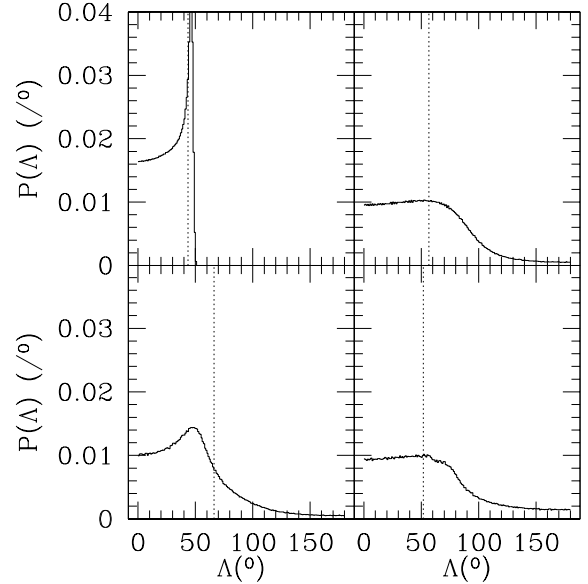


FIG. 31.— The long-term Λ distribution of the same 4 *v* And simulations as in Fig. 30. *Top Left*: This Λ distribution is typical of a regular system. *Other Panels*: The distributions are typical of chaotic configurations. From these plots we conclude the secular resonance locking is important in maintaining stability, or regularness in *v* And.

4.2. 47UMa

The 47UMa system consists of a $1.03 \pm 0.03 M_\odot$ (Gonzalez 1998) star and 2 interacting companions: b and c, at 2.09AU and 3.73AU respectively. The initial eccentricities in this system are substantially lower than *v* And at 0.06 and 0.1⁵ respectively. More recent measurements place e_c much closer to 0. However, “ $e_c=0.3$ provides almost as good a fit to the radial velocity data as does $e_c=0.005$ ” (Laughlin, Chambers, & Fischer 2002). Should $e_c \leq 0.1$ then, of all the systems examined in this paper, 47UMa most closely resembles our own. Planet b is the larger planet and hence determines $\tau_{47UMa}=840,000$ years.

Overall $80.3 \pm 4.7\%$ of simulations were stable over τ_{47UMa} . This is less than a 2σ difference from *v* And. In unstable configurations planet c, the less massive planet, was ejected every

⁵<http://exoplanets.org>

Table 8 - Results of Long Term (10^8 yr) Simulations of v And

| Trial | $e_{c,0}$ | $e_{d,0}$ | R_0 | Λ_0 ($^\circ$) | ϵ | Result ^a |
|-------|-----------|-----------|-------|--------------------------|------------------------|--------------------------------|
| 006 | 0.302 | 0.345 | 5.351 | 43.6 | 2.1×10^{-9} | R |
| 007 | 0.438 | 0.371 | 5.375 | 7.8 | 0.093 | C, $\epsilon(2.6)$, E(b,2.7) |
| 054 | 0.145 | 0.201 | 5.559 | 56.6 | 1×10^{-8} | C |
| 109 | 0.392 | 0.411 | 5.28 | 43.4 | 0.32 | C, $\epsilon(3.2)$, E(c,79.4) |
| 152 | 0.253 | 0.348 | 5.378 | 48.2 | 2.1×10^{-8} | R |
| 164 | 0.0938 | 0.128 | 5.422 | 46.4 | 9.5×10^{-9} | R |
| 192 | 0.252 | 0.342 | 5.448 | 51.8 | 3.9×10^{-5} | C, E(b,54.8) |
| 288 | 0.348 | 0.389 | 5.227 | 66.2 | 1.2×10^{-6} | C |
| 499 | 0.256 | 0.349 | 5.369 | 1.1 | 5.2×10^{-9} | R |
| 880 | 0.242 | 0.343 | 5.138 | 16.7 | 1.6×10^{-8} | R |
| 989 | 0.245 | 0.305 | 5.431 | 26.0 | 1.075×10^{-4} | C, $\epsilon(77.3)$ |

^a R=Regular, C=Chaotic, ϵ =Energy conservation failed (Time (10^6 yr)), P=Perturbed (Planet, Time (10^6 yr)), E=Ejected (Planet, (10^6 yr))

time. This is similar to ν And in which the most massive planet perturbed the smaller planets. The instability rate as a function of time is presented in Fig. 32. The rate for 47UMa is similar to the other systems in that most unstable configurations perturb a planet past stability on relatively short timescales, but with a tail to longer times. The rate does not reach zero, however, and suggests that more unstable configurations exist.

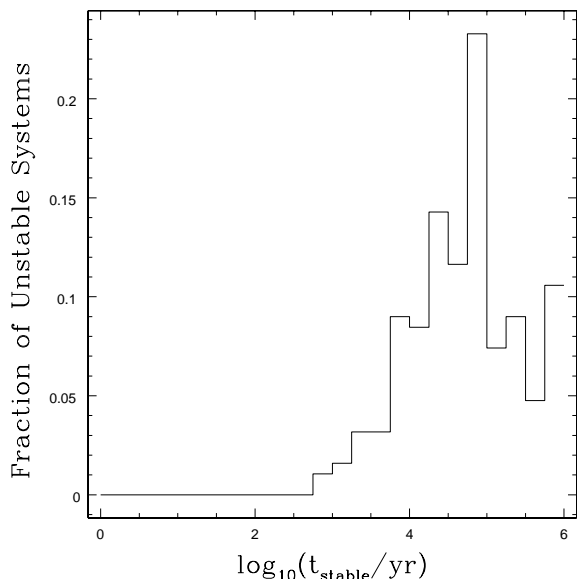


FIG. 32.— Instability rate in 47UMa. Most ejections occur at 10,000 to 100,000 years. In this system, even unstable configurations generally survive for at least 10,000 years.

The 47UMa stability map is presented in Fig. 33. The overall structure of stability in eccentricity space is qualitatively the same as in ν And, with one major exception: stability is correlated with e_2 (e_c), not e_1 (e_b). The errors for e_c are substantial. The main difference between 47UMa and ν And is that the more massive companion is the interior planet. This configuration makes it more difficult for the exterior planet to perturb the interior planet which is more tightly bound to the parent star.

This stability map is in good agreement with other work done on this system. Using MEGNO, Goździewski (2002) determined the maximum value for e_c to be approximately 0.15. A stability analysis in Laughlin, Chambers, & Fischer (2002) also shows a similar dependence on e_c . For nearly coplanar systems, such as those presented here, they determined the maximum value for e_c to be less than 0.2. Although the exact maximum value for e_c is different for all three studies, it is clear that the value of e_c determines stability for 47UMa.

When comparing Fig. 33 with Fig. 22, we see that the edge in the ν And system is much cleaner than in 47UMa. One possible reason for this is the system's proximity to the 5:2 mean motion resonance. To examine this possibility, in Fig. 34 we plot stability as a function of R in this system. Although there appears to be some increase in stability beyond 5:2, and a decrease inside 5:2, the errors are too large to confirm that this is a real effect.

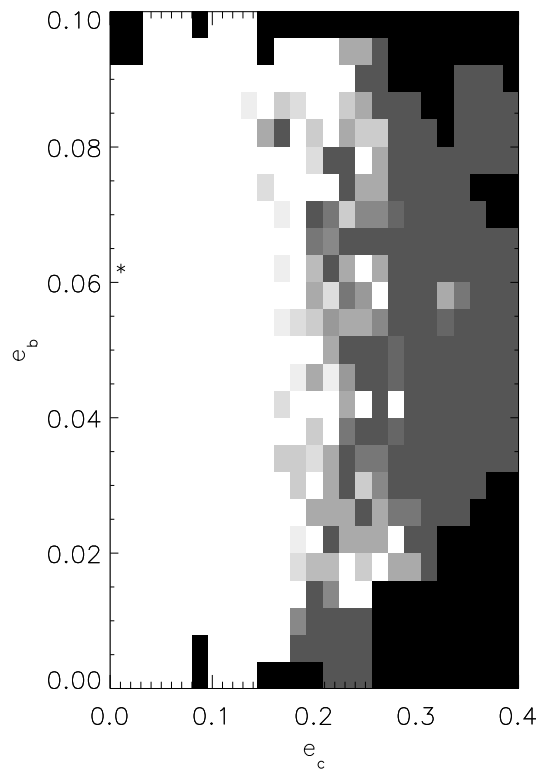


FIG. 33.— The stability map for 47UMa. The relevant orbital elements are e_b and e_c . For this system the value of e_c determines stability. The current best fit to this system, as of 1 Nov 2002, is marked by the asterisk (Laughlin, Chambers, & Fischer 2002). Note that although this system appears to lie far from the edge, the observational error for e_c is ± 0.115 .

In Figs. 35-37 we examine several possible orbital evolutions for 47UMa. Some sample simulations from the suite of 1000 are listed in Table 9. First, in Fig. 35, is a stable regular configuration. Over 50% of all configurations for this system are regular. In this case the eccentricities, and inclinations show very small oscillations (10%) and Λ librates with an amplitude of 45° .

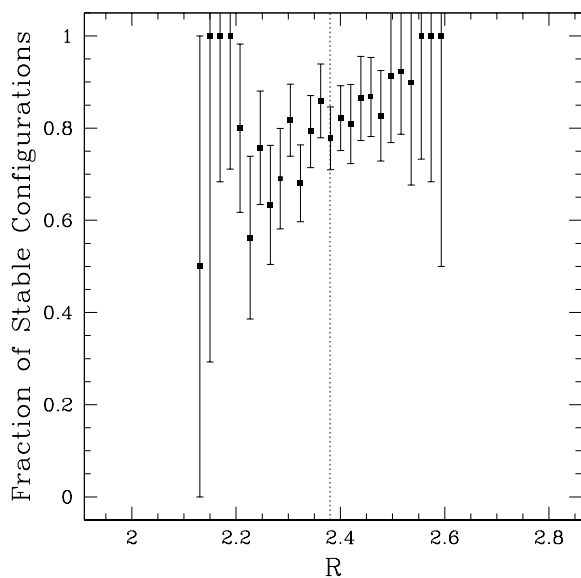


Table 9 - Selected Simulations of 47UMa

| Trial | $e_{b,0}$ | $e_{c,0}$ | R_0 | Comments ^a |
|-------|-----------|-----------|-------|-------------------------|
| 006 | 0.021 | 0.211 | 2.384 | C, P(c,21.5), E(c,38.1) |
| 025 | 0.043 | 0.077 | 2.503 | C |
| 032 | 0.065 | 0.105 | 2.405 | R |

^a R=Regular, C=Chaotic, P=Perturbed(Planet, Time (10^3 yr)), E=Ejected(Planet, Time (10^3 yr))

FIG. 34.— The stability of 47UMa as a function of R . This system lies very close to the 5:2 mean motion resonance. There is some indication of more stability exterior to 5:2, and less interior, but the statistics are not robust enough to confirm this. The dashed line represents the current best fit to the system.

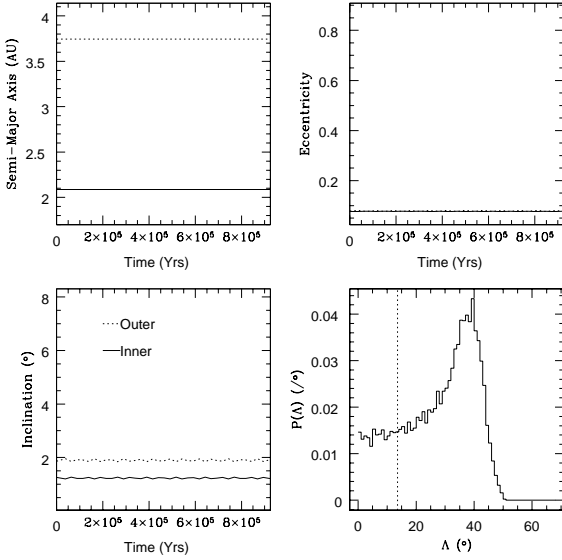


FIG. 35.— The orbital evolution of 47UMa-032, a stable, regular configuration of 47UMa. The data are smoothed on 25,000 year intervals. *Top Left*: The semi-major axes show no hint of perturbations. *Top Right*: The eccentricities vary on a 4800 year timescale for the duration of the simulation. *Bottom Left*: This system never deviates more than 5° from coplanarity. The inclinations oscillate on a 4400 year period. *Bottom Right*: In this configuration Δ is aligned, but librates with an amplitude of 45° .

As with all other systems, there are chaotic, but stable examples of 47UMa. One such system, 47UMa-025, is examined in Fig. 36. The semi-major axes of this configuration show no signs of perturbations, but the eccentricities and inclinations show clear signs of chaos, though no perturbation is very large. As with stable, chaotic configurations of other systems, circulation appears to be the dominant mode of Δ evolution. However, this system is actually librating about an anti-aligned orientation, with only occasional circulation. The amplitude of this libration is quite variable, sometimes as high as 165° .

In Fig. 37, we present an example of the ejection of planet c. This system evolves regularly for 10,000 years, then experiences 25,000 years of chaotic evolution, culminating in the ejection of the outer planet. For this configuration Δ circulates during the first 30,000 years, both regular and chaotic epochs, but with different angular velocities in each stage. During the final 10,000 years, however, when e_c becomes very large, Δ becomes locked at 155° .

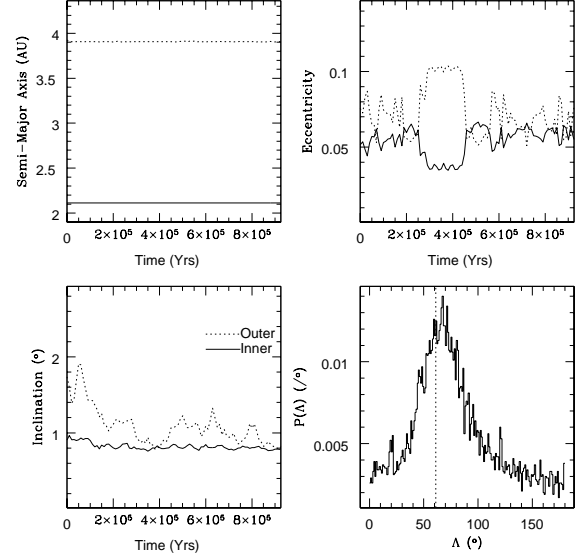


FIG. 36.— The orbital evolution of 47UMa-025, a stable, chaotic configuration of 47UMa. *Top Left*: The semi-major axes show no hint of perturbations. *Top Right*: The eccentricities vary by only 25% for the duration of the simulation, but show clear coupled, chaotic behavior. *Bottom Left*: This nearly coplanar simulation also shows obvious chaos in the evolution of the inclinations. *Bottom Right*: This Δ distribution function is libration about anti-alignment with an amplitude which varies between 100° and 165° , but also with occasional circulation.

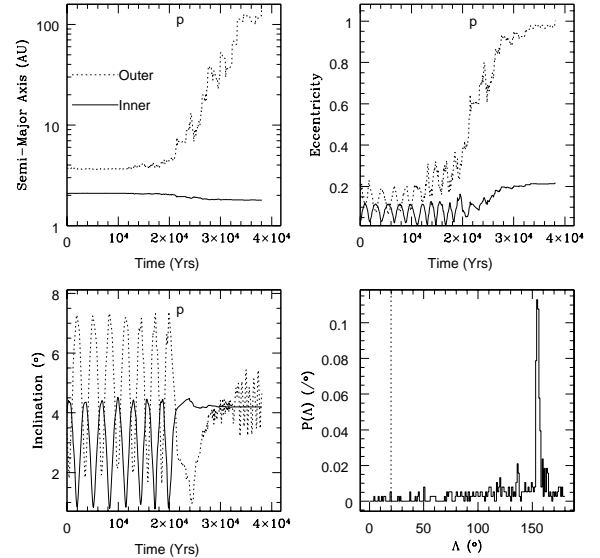


FIG. 37.— The orbital evolution of 47UMa-006, a chaotic, unstable configuration of 47UMa. The p marks the time that our perturbation criterion is met. *Top Left*: The semi-major axes evolve quiescently for 10,000 years, then e_c begins its slow trek to upward of 200AU. The system is perturbed, however, until 21,500 years. Note that the y-axis is logarithmic in this example. *Top Right*: After 10,000 years, the system suddenly becomes chaotic, eventually pushing e_c to unity in 40,000 years. *Bottom Left*: As with the eccentricities, the inclinations evolve regularly for 10,000 years, but then become chaotic. *Bottom Right*: In this configuration Δ circulates, but eventually becomes locked at 155° for the final 10,000 years.

Table 10 - Results of Long Term (10^9 yr) Simulations of 47UMa

| Trial | $e_{b,0}$ | $e_{c,0}$ | R_0 | Λ_0 ($^\circ$) | ϵ | Result ^a |
|-------|-----------|-----------|--------|--------------------------|----------------------|---------------------|
| 238 | 0.0587 | 0.0809 | 2.4006 | 124.0 | 4×10^{-6} | R |
| 257 | 0.0637 | 0.0169 | 2.3737 | 57.7 | 3.7×10^{-6} | R |
| 307 | 0.0594 | 0.115 | 2.4312 | 122.6 | 1.9×10^{-6} | R |
| 355 | 0.0577 | 0.0887 | 2.4332 | 64.3 | 4.2×10^{-6} | R |
| 507 | 0.0607 | 0.111 | 2.4498 | 40.8 | 3.4×10^{-6} | R |
| 546 | 0.063 | 0.113 | 2.3402 | 6.1 | 4.3×10^{-6} | R |
| 624 | 0.0595 | 0.118 | 2.5513 | 164.5 | 3.4×10^{-6} | C |
| 633 | 0.0583 | 0.0900 | 2.4872 | 94.3 | 4×10^{-6} | R |
| 792 | 0.062131 | 0.0897 | 2.3957 | 88.2 | 2×10^{-6} | R |

^a R=Regular, C=Chaotic

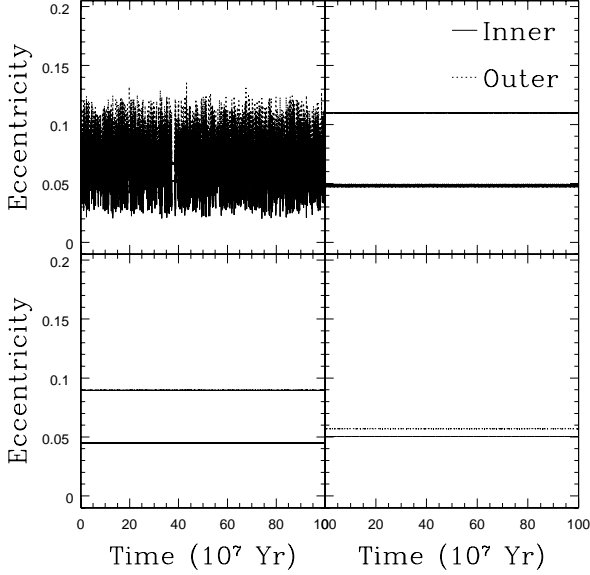


FIG. 38.— Eccentricity evolution of 4 long term simulations of 47UMa. *Top Left*: Evolution of 47UMa-624. *Top Right*: Evolution of 47UMa-307. *Bottom Left*: Evolution of 47UMa-238. *Bottom Right*: Evolution of 47UMa-257. Most systems are regular for the duration of the simulation. However the top right is clearly chaotic, yet it still survives for 10^9 years.

Long term simulations of 47UMa were integrated for 10^9 years. Table 10 is a summary of all long term simulations for 47UMa. Fig. 38 shows the eccentricity evolution of 4 systems. The top right panel of this figure is fascinating. The system is very chaotic for the first 350 million years, then enters a short (~ 20 million years) period of quiescence, only to return again to a similar chaotic state. The other configurations all appear regular. Fig. 39, plots the Λ evolution. In 47UMa no secular resonance locking occurs. However these plots confirm the results of Laughlin, Chambers, & Fischer (2002). They show that for low values of e_c (< 0.1) the system should librate in an aligned configuration, but above 0.1 the system should be anti-aligned. The chaotic case, as expected, has a flat distribution function.

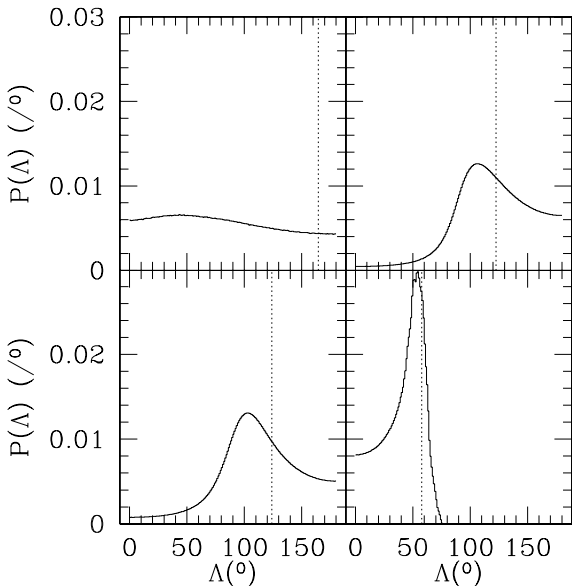


FIG. 39.— The distribution of Λ for 4 stable long term simulations of 47UMa. The chaotic system (top left) shows a nearly flat distribution in Λ . This suggests that Λ is behaving chaotically as well. Two regular systems (top right, and bottom left) show libration about anti-parallel configurations, whereas the bottom right librates about $\Lambda = 0$.

4.3. Gas Giants

Perhaps the most interesting aspect of the new ESPS is their comparison to the SS. The procedure outlined in §2 permits a comparison of the ESPS and the SS. We must first, however, determine how to vary the initial conditions of the gas giants. As can be seen in Table 6, the “error” associated with each planet is arbitrary. We have given a spread in initial conditions that is roughly similar to the percent error as listed in the ESPS. For example the periods are allowed to vary by approximately 10%, but the eccentricities have a standard deviation of 0.1 for all planets. This procedure will allow us to create a stability map for the SS, but will make a comparison of the probabilities of survival less meaningful.

The outer SS consists of 4 gas giants located between 5.2 and 40AU. The gas giants are on much more circular orbits than the ESPS planets (Saturn has the largest eccentricity at just over 0.05). Because of the large semi-major axes, τ_{SS} corresponds to 3.32×10^6 years. Compared to known ESPS the gas giants are relatively low-mass planets. In fact Uranus and Neptune could not be detected via the Doppler method at the precision level currently achieved (see §4.4).

Chaos in the SS is well documented (e.g. Sussman & Wisdom 1988, Sussman & Wisdom 1992, Varadi *et al.* 1999, Lecar *et al.* 2001). In fact Varadi *et al.* (1999) show that the Jupiter-Saturn system lies very near chaotic regions. They vary the semi-major axes of these two planets slightly (less than 1%) and find that this is enough to identify broad chaotic regions. Below we show that by enlarging this variation, the system moves into total instability; ejections are inevitable.

For the gas giants $85.3\% \pm 4.3\%$ of the trials were unperturbed for 3.3×10^6 years. In Paper I, we integrated 32 gas giant configurations. Of these 81% survived. As in §4.1 we again recover the results of Paper I. In this system Jupiter was never ejected; it always removed the other planets from the system. Saturn was ejected in 14% of the simulations, Uranus, (the least massive) 62%, and Neptune, 24%. In the SS therefore, ejection rate is tightly coupled to mass, as was observed in the other ESPS. It therefore seems that the SS behaves like other interacting systems.

Fig. 40 is the instability rate. Most configurations survive for 10^5 years. Once again it appears the perturbation rate does not fall to zero, and we note that this means that we have not found all the unstable systems. The last bin in this plot contains only 20,000 years worth of data. It is therefore unclear if the ejection rate might still be rising with larger time. Should that be the case that our choice for τ_{SS} is too small, and suggests that we have not identified all unstable configurations. Fig. 41 is the stability map for the gas giants. The gas giants show a plateau as in 47UMa and in ν And, however the edge is much less dramatic. The actual values for our gas giants shows that our system lies quite far from the stability edge. We also note that the stability plateau shows many depressions, and the abyss contains many spires. This apparent difference between the SS and other interacting systems may result from not determining all unstable configurations. Perhaps longer integrations would sharpen the edge, and broaden the instability abyss. Dynamically speaking the major difference between the SS and other

interacting systems is that the SS has a much broader range of orbital times. Jupiter orbits 13 times more quickly than Neptune. Perhaps instability is more relevant on timescale based on the orbit of Neptune (see §6). However these features may also arise from the system’s proximity to the 5:2 resonance, the so called “Great Inequality”. We address this possibility in §4.4.

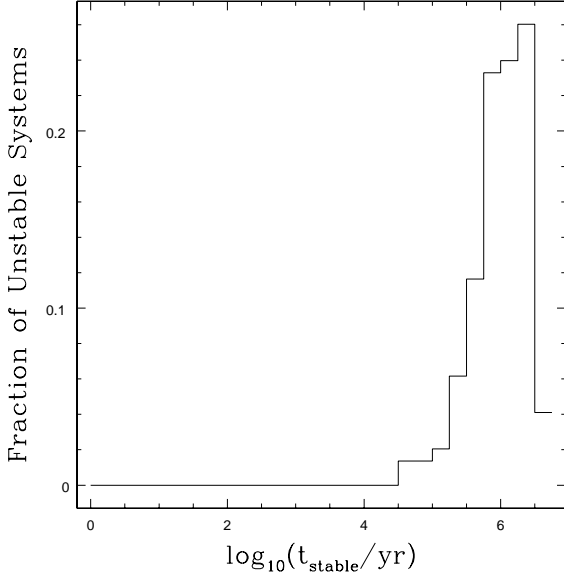


FIG. 40.— Rate of instability in the SS. Instability requires at least 30,000 years to develop, and continues through τ_{SS} .

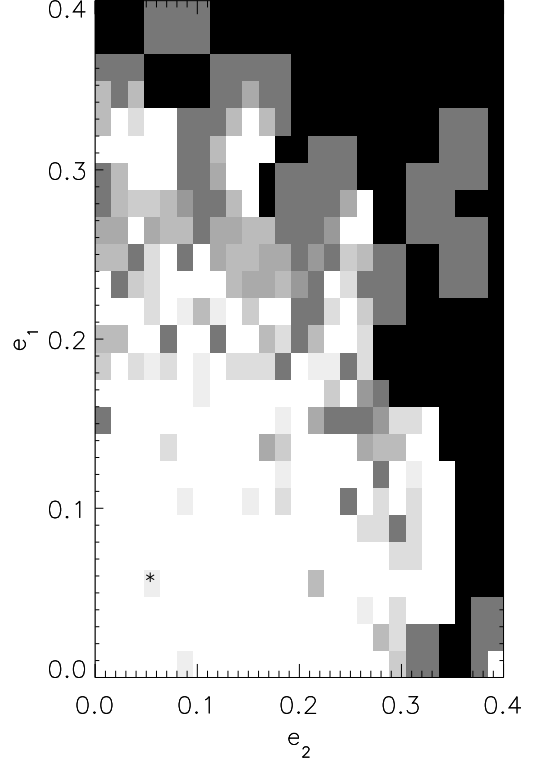


FIG. 41.— Stability map for the gas giants. In eccentricity space, the SS lies near a small depression. The edge in the gas giant system is not nearly as clean as in other interacting systems. This may be because our choice of τ is too low to find most unstable configurations.

Several example simulations are shown in Figs. 42–47. The initial conditions and outcomes of these simulations are shown in Table 11. A regular, stable example is shown in Fig. 42. The eccentricities and inclinations are a linear superposition of eigenmodes. Although Λ begins nearly anti-aligned, it quickly moves into a large amplitude librational mode. The circulation, which is typically an indicator of chaos, appears to not influence the eccentricity evolution.

The best fit to e_J , e_S and R is simulation SS-183. The orbital evolution of this system is shown in Fig. 43. Note, however, that Λ_0 differs substantially from its standard value of 68.5° . This difference is responsible for the chaotic evolution of e_J and e_S . Curiously, though, the evolution of e_U and e_N are regular. Unlike the eccentricities, all the inclinations evolve regularly. The nodes of Uranus and Neptune librate about anti-alignment, but with occasional circulation. Note that in e and i Uranus oscillates from 2 modes, whereas Neptune experiences 3 modes.

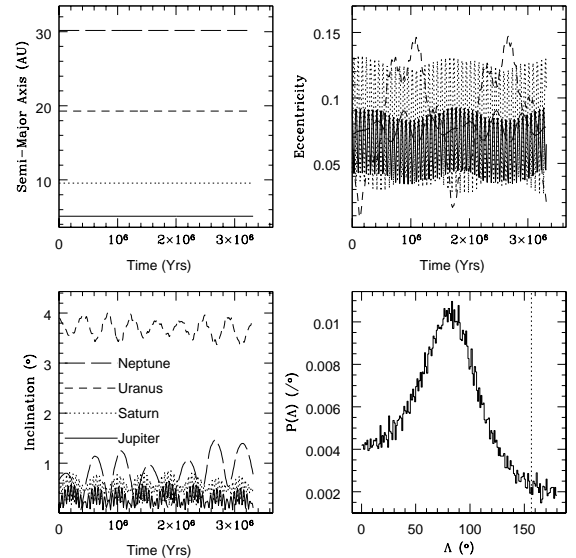


Table 11 - Selected Simulations of the Gas Giants

| Trial | $e_{J,0}$ | $e_{S,0}$ | R_0 | Comments ^a |
|-------|-----------|-----------|-------|-----------------------|
| 157 | 0.155 | 0.042 | 2.40 | C, E(N,2.8) |
| 180 | 0.155 | 0.0095 | 2.45 | C, E(U,2.1) |
| 183 | 0.056 | 0.055 | 2.48 | R/C |
| 278 | 0.0944 | 0.223 | 2.45 | C, E(S,0.66) |
| 306 | 0.124 | 0.230 | 2.46 | C |
| 402 | 0.093 | 0.203 | 2.55 | R |

^a R=Regular, C=Chaotic, E=Ejected(Planet, Time (10^6 yr))

FIG. 42.— The orbital evolution of SS-402, a stable, regular configuration of the gas giants. The 4 planetary bodies in this system result in more complicated dynamics as the smaller 2 planets often experience several modes of oscillation. *Top Left*: The semi-major axes do not change for the duration of the simulation. *Top Right*: The eccentricities are combinations of sinusoids. Jupiter and Saturn both oscillate on a 70,000 year period. Uranus and Neptune vary on a 1.5 million year timescale. Their motion however also has 4 million year mode, due to beating with the oscillations from Jupiter and Saturn. *Bottom Left*: All the inclinations evolve as a function of two modes. Jupiter and Saturn oscillate on a 40,000 year cycle. Uranus and Neptune oscillate on a 500,000 year period. As with eccentricity we observe beating between these 2 frequencies in all planets. *Bottom Right*: Λ switches between libration with a 80° amplitude, and circulation.

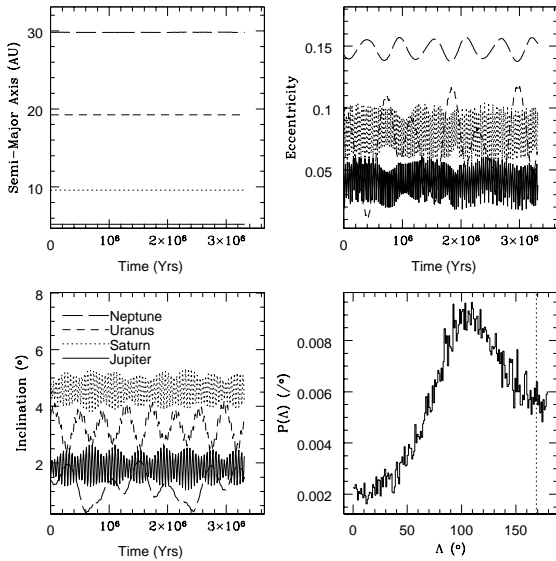


FIG. 43.— The orbital evolution of SS-183, a stable configuration of the gas giants in which some elements evolve regularly, others chaotically. *Top Left*: The semi-major axes do not change for the duration of the simulation. *Top Right*: The eccentricities of Jupiter and Saturn evolve chaotically, but Neptune and Uranus appear to be regular. *Bottom Left*: All inclinations evolve regularly, although the number of modes is different, Jupiter, Saturn, and Neptune have 2 modes, but Uranus has 3. *Bottom Right*: Λ shows the typical distribution function of libration about anti-alignment and circulation. This alternating results in the chaotic evolution of e_J and e_S through $e-\varpi$ coupling.

In Fig. 44 a fully chaotic, yet stable configuration is shown. The semi-major axes show obvious signs of encounters, but never change by more than 20%. The eccentricities are very chaotic, but rarely reach 0.3. The inclinations, too, are extremely chaotic, but never surpass 12° . The double peaked Λ distribution function is another clear indicator of chaos.

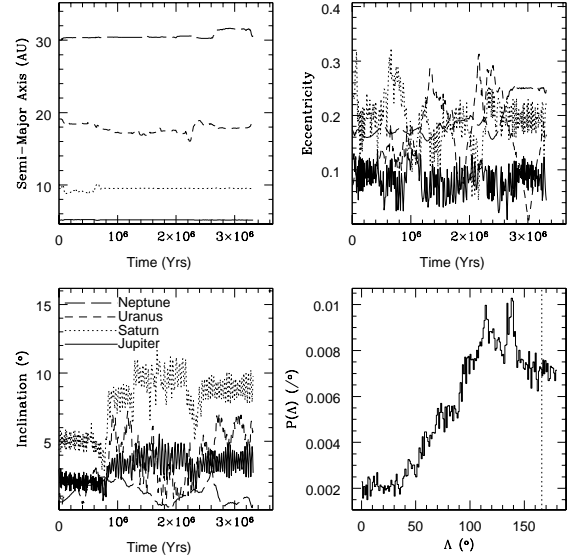


FIG. 44.— The orbital evolution of SS-306, a stable, chaotic configuration of the gas giants. *Top Left*: The semi-major axes begin migrating immediately, but a change greater than 20% does not occur for the duration of the simulation. *Top Right*: All eccentricities undergo chaotic oscillations, but the amplitudes are small. No eccentricity ever reaches 0.35. *Bottom Left*: The inclinations also evolve chaotically with low level oscillations. The system remains close to coplanarity, as i_S never exceeds 12° . *Bottom Right*: This Λ distribution is clearly chaotic as the 2 peaks and circulation demonstrate.

In Fig. 45 we present an example of the ejection of Saturn. Although the semi-major axes show obvious signs of perturbations, it is only during the last 50,000 years that any planet's semi-major axis changes by more than 10%. The eccentricities and inclinations do not show large fluctuations until Saturn is quickly ejected after 65,000 years.

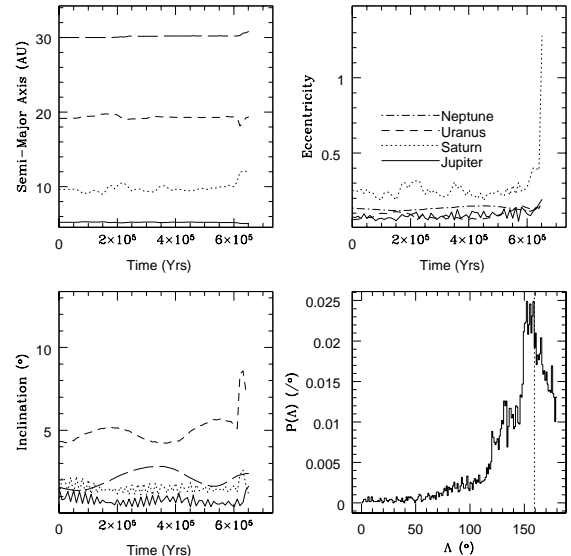


FIG. 45.— The orbital evolution of SS-278, the ejection of Saturn. *Top Left:* The semi-major axes deviate from the initial values by less than 10% until the final 50,000 years of integration. Even then a_S only increases by 15%. *Top Right:* All eccentricities are chaotic, but the values remain close to their initial conditions until Saturn is thrown from the system. *Bottom Left:* The inclinations appear to evolve regularly for 35,000 years until Jupiter and Saturn become chaotic. Uranus becomes chaotic after 60,000 years, but Neptune remains regular for the duration of the simulation. *Bottom Right:* The Λ distribution for this configuration is quite unusual and also indicates the system is chaotic.

The ejection of Uranus is shown in Fig. 46. The semi-major axes of Jupiter and Saturn remain nearly constant throughout the simulation, but Neptune and Uranus are clearly interacting. The eccentricities are chaotic, but remain near the starting values, except for Uranus, which steadily increases until it is ejected after 2×10^6 years. The inclinations are also chaotic. Jupiter and Saturn appear to have 1 normal mode, and 1 chaotic mode, while Neptune and Uranus are fully chaotic. The longitudes of periastron tend to remain near alignment, but the 3 peaks clearly bely the chaos in the system.

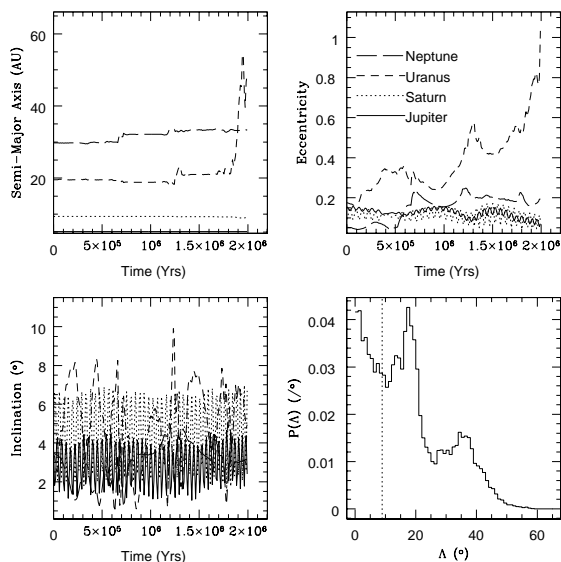


FIG. 46.— The orbital evolution of SS-180, the ejection of Uranus. *Top Left:* The semi-major axis of Jupiter does not change, and Saturn changes by less than 0.1AU at the very end of the simulation. Uranus and Neptune are clearly interacting, but the fluctuations of e_U and e_N are small until 1.75×10^6 years. *Top Right:* While the eccentricities of Jupiter, Saturn, and Neptune remain low, Uranus's eccentricity gradually grows until it is ejected after 2×10^6 years. *Bottom Left:* The inclinations all also show chaos, but Jupiter and Saturn appear to have a regular 3000 year mode superimposed on small chaotic fluctuations. *Bottom Right:* The Λ distribution for this configuration is quite unusual and also indicates the system is chaotic. Note, however, that the system is experiencing a generic form of libration, as Λ never exceeds 60° .

Finally we plot the evolution of a configuration that ejects Neptune in Fig. 47: SS-157. After 750,000 years Uranus becomes the most distant planet. After Uranus and Neptune have a close approach which flings Neptune from the system, Uranus drops to a 15AU orbit. It is likely that it would then encounter Saturn, and another planet would be removed from the system. Despite the large variations in semi-major axes, the eccentricities remain relatively calm. Jupiter and Saturn in particular appear nearly regular. In inclination, they in fact are regular.

For all the unstable cases shown here, this configuration's Λ shows the least chaos. Although there is some flipping between a librational and a circulation mode. Λ also demonstrates that the chaos between Neptune and Uranus does not affect the evolution of Jupiter and Saturn's orbits.

These last three figures reveal why the stability map for the SS is different than for other interacting systems. Sometimes, even when e_J and e_S are low, the smaller bodies in the system can interact with each other violently. Although the eccentricity of Jupiter and Saturn are generally the most important factor in system stability. The larger the values of any eccentricity, the more likely is instability.

We ran no long term simulations on the SS. The orbital elements for the SS are well determined, and many long term simulations have already been performed on this system (see Duncan & Quinn 1993, Lecar *et al.* 2001).

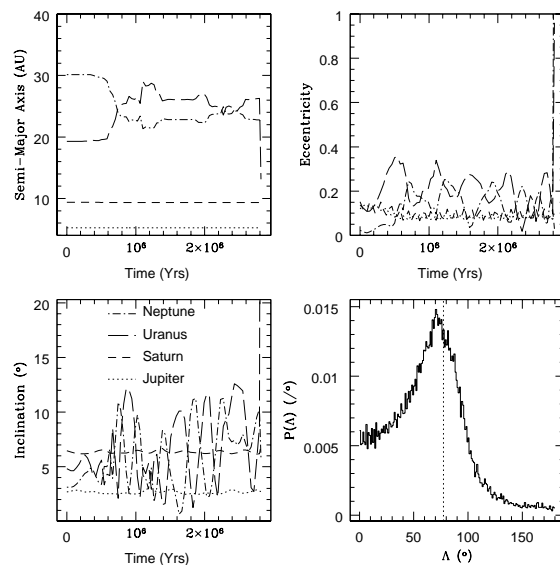


FIG. 47.— The orbital evolution of SS-157, the ejection of Neptune. These data are smoothed over a 40,000 year interval. *Top Left:* After 750,000 years Neptune and Uranus cross orbits, and Uranus becomes the most distant planet. After ejecting Neptune Uranus drops to a 15AU orbit which would most likely encounter Saturn relatively quickly and result in another ejection. Jupiter and Saturn remain on regular orbits. *Top Right:* All eccentricities remain low for the duration of the simulation until Neptune is removed after 2.8×10^6 years. This is true even while Uranus and Neptune are in 1:1 resonance at 750,000 years and 2.2 million years. Jupiter and Saturn experience sinusoidal oscillations throughout the simulation. *Bottom Left:* The inclinations of Jupiter and Saturn are regular but Uranus and Neptune are clearly chaotic. Note that the encounter that throws Neptune from the system sends Uranus into a highly inclined orbit. *Bottom Right:* For this configuration Λ is generally librating in an aligned state with an amplitude of 70° , but with some circulation.

4.4. Jupiter and Saturn

As mentioned above Uranus and Neptune do not provide enough reflex velocity, K , motion in the star to be observable by current technology ($K \sim 3\text{m/s}$). Should any planet of Uranus or Neptune mass exist in the observed ESPS they would not be detected. Therefore we followed the same procedure with just Jupiter and Saturn. This suite of simulations can also provide clues as to how other ESPS will behave if they have additional, distant companions.

Not surprisingly this 3-body system is more stable than the 5-body system, as $96.3 \pm 2.4\%$ of the trials remained stable. In this system Jupiter was ejected 6.9% of the time, and Saturn 93.1%. It seems as though instability is being passed through Saturn and into the smaller planets. We can therefore apply this result to the other ESPS. This Jupiter-Saturn system is analogous to the 47UMa system. The mass ratio of the planets are about the same, as is R . The only substantial difference is that the masses are higher and the orbits closer in 47UMa. However, our simulations of 47UMa used $e_c=0.1$. This is about twice as high as e_{Saturn} . This decrease in eccentricity is clearly important as the Jupiter-Saturn system is substantially more stable than 47UMa. This again demonstrates that the eccentricities of the planets are key in determining stability.

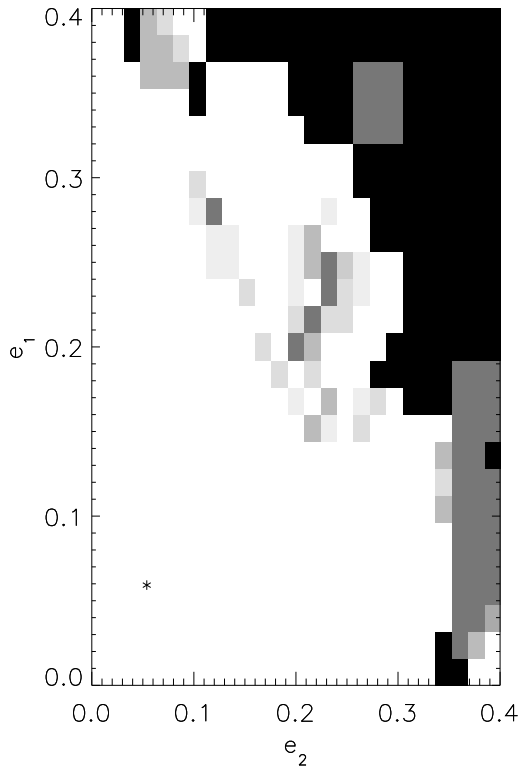


FIG. 48.— Stability map for the Jupiter-Saturn system. This map shows some similarities to that for the gas giants (see Fig. 44). The line demarcating the plateau follows approximately the same diagonal line. As well we still see a few depressions in the plateau.

Fig. 48 is the stability map for the Jupiter-Saturn system. This plot is similar to Fig. 41. There is a boundary at approximately the same location in eccentricity space, however the drop is not so sharp, nor as deep as in the gas giant system. Further an additional plateau rises at larger eccentricities. This last phenomenon is not observed in any other system in this paper.

As mentioned in §4.3, stability might be correlated with the 5:2 resonance. Fig. 49 shows stability as a function of R for the SS. There is a hint that as the system moves out of this third order resonance, stability increases, but the errors on these distant configurations are too large to confirm this possibility. In 47UMa $R = 2.38$, while in the SS, $R = 2.48$. Although there are no statistically meaningful points in Figs. 34 and 49, the same

trend appears in both. Namely that interior to 5:2 instability is more prevalent. As has been shown throughout this paper, the eccentricities determine the overall stability, and the statistics are too poor to claim any trend with R in either system.

Comparing the gas giants with Jupiter-Saturn provides us with an excellent opportunity to explore completeness. As mentioned above, the Jupiter-Saturn system is similar to 47UMa, yet the stability maps are quite different. The Jupiter-Saturn system is the only system examined with no instability abyss, and it is the only system we know to be incomplete.

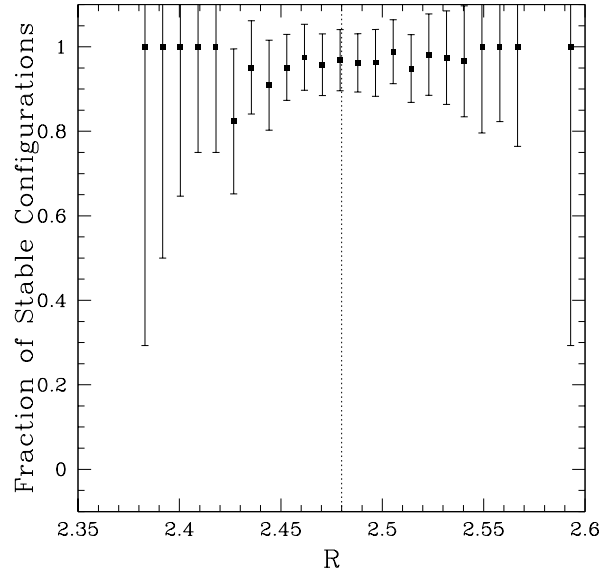


FIG. 49.— Stability as a function of R for the Jupiter-Saturn system. As in 47UMa there is a hint that instability increases inside the 5:2 resonance; no data point lies more than 1σ from the mean rate of stability (96%). It therefore appears that this resonance has minimal impact on the system. The dashed vertical line represents the true value of R in the SS.

5. SEPARATED SYSTEMS

By the end of 2002 three separated systems had been announced: HD83443⁶, HD168443 (Marcy *et al.* 2001b), and HD74156⁷. The values and errors for these systems are reproduced in Table 12. HD83443 consists of 2 Saturn mass planets in very tight orbits. HD168443 consists of 2 very large companions ($m_1 \geq 17M_{\text{Jup}}$, $m_2 \geq 7.5M_{\text{Jup}}$). In fact planet c should be considered a brown dwarf, and if the system is more inclined than 35 degrees planet b would also be a brown dwarf. For this system $R = 30.5$. HD74156 contains 2 bodies of slightly more than a Jupiter mass, with $R = 44.6$. We only examined HD168443 and HD83443. Evidence is mounting that HD83443 is not a multiple system (Butler *et al.* 2002), therefore we stopped the simulations on this system after 847 trials had been completed. For HD168443 and HD83443, all simulations survived to τ . HD74156 has a larger R , and smaller masses than HD168443. It therefore seems highly doubtful that any simulation of HD74156 would produce an unstable configuration.

Although all simulations were stable, the dynamics of HD168443 are still interesting. The eccentricities and inclinations of this system show a weak planet-planet interaction. Although no evidence of chaos is evident, the planets apparently

⁶http://obswww.unige.ch/~udry/planet/hd83443_syst.html

⁷<http://obswww.unige.ch/~udry/planet/hd74156.html>

Table 12 - Initial Conditions for Separated Systems

| System | Planet | Mass(M_J) | Period(d) | Eccentricity | Long. of Peri.(Deg) | Time of Peri. (JD) |
|----------|--------|---------------|---------------------|-------------------|---------------------|-----------------------|
| HD168443 | b | 7.73 | 58.1 ± 0.006 | 0.53 ± 0.003 | 172.9 ± 0.4 | 2450047.58 ± 0.2 |
| | c | 17.15 | 1770 ± 25 | 0.20 ± 0.01 | 62.9 ± 3.2 | 2450250.6 ± 18 |
| HD74156 | b | 1.56 | 51.619 ± 0.053 | 0.649 ± 0.022 | 183.7 ± 3.3 | 2451981.4 ± 0.57 |
| | c | 7.3 | 2300(Fixed) | 0.395 ± 0.074 | 240 ± 12 | 2450819 ± 75 |
| HD83443 | b | 0.34 | 2.9853 ± 0.0009 | 0.079 ± 0.033 | 300.25 ± 17.05 | 2451386.5 ± 0.14 |
| | c | 0.16 | 29.83 ± 0.18 | 0.42 ± 0.06 | 337.42 ± 10.42 | 2451569.59 ± 0.73 |

are close enough that they feel each other. This system may be fully stable, but it appears to lie close to the boundary between interacting and separated systems. We hypothesize that this proximity to interacting systems is due to the large planetary masses in this system.

6. SUMMARY

In this paper we have described the dynamics of three different morphological classifications of planetary systems. We find that the systems in each of the classifications have similar stable regions. In resonant systems very small stability zones exist in phase space, and stability is tightly coupled with R and, to a lesser degree, e_1 , where e_1 is the eccentricity of the most massive companion. In interacting systems, the zones are larger, but are correlated with e_1 and e_2 , where e_2 is the eccentricity of the second most massive companion. In these systems we see a correlation with eccentricity and the location of the most massive planet. Large interior planets are almost impossible to eject (47UMa, the gas giants), whereas large exterior planets can be ejected sometimes (ν And). Separated systems are completely stable as observed.

Table 13 summarizes the results of this paper. In this table f_{stable} is the fraction of configurations that were stable, and $f_j, j = 1, 2, 3, \dots$ is the fraction of unstable systems which perturbed/ejected that planet. Note that the subscripts correspond to mass, not semi-major axis (1 being the most massive companion). We therefore strengthen the theory suggested in Paper I: all interacting planetary systems lie near the edge of stability.

There are some obvious similarities among the systems. One particularly intriguing result is the similarity in f_{stable} between systems in the same classification. Resonant systems have survival probabilities less than 20%, whereas interacting systems lie close to 80% and the separated systems are completely stable. Of the interacting systems, 47UMa stands out as being far from the stability edge.

The choice of $\tau = 2.8 \times 10^5 P_1$ appears to identify most unstable configurations. For both resonant systems $\tau < 10^6$ yrs, but since the simulations were integrated to 10^6 yrs we may estimate the usefulness of this arbitrary value. For both GJ876 and HD82943 approximately 2-3% of configurations ejected a planet after τ . For the ν And system, 1.5% of unstable systems were ejected in the last bin of Fig. 20. For 47UMa the rate was over 10%, and for the SS the rate was 4%. However as was noted in §4.3, this low rate for the SS may be the result of poor sampling in the last bin. Although all these systems reached a maximum ejection rate before τ , the nonzero rate at τ demonstrates that our choice for τ was slightly too short. In GJ876 some ejections occurred right up to 10^6 yrs, but by 10^4 yrs ($0.25\tau_{GJ876}$) over 90% of unstable cases had been identified. The situation is nearly the same for HD82943; 90% of unstable cases were identified by 30,000 years ($0.1\tau_{HD82943}$), but ejections continued for 10^6 years. Given these statistics, a better choice for τ would be $\tau = 10^6 P_{outer}$. However, it is important to note that instability can arise after this, as is shown in Figs. 9, 18, and 30. The simulations presented here clearly demonstrate the unpredictable behavior of chaotic systems; no choice of τ would identify all unstable configurations. One should therefore note that all the global results presented here are upper limits. The probability of survival and extent of stable phase space are smaller than what is shown here.

Long term simulations ($\geq 10^8$ orbits) show that all systems have regular configurations on this timescale. However only one simulated configuration of GJ876 showed this behavior.

Some configurations may show a large degree of chaos for up to 10^9 years (see Fig. 38, top left), eject a planet after an arbitrarily long period of time (Fig. 30, bottom right), in addition to quiescent, regular evolution. Regular orbits tend to librate about $\Lambda=0$, but this is not necessary for stability (see Figs. 10, 19, 31, and 39).

7. DISCUSSION

Ideally this research provides insights into planet formation. In particular, the current distribution of orbits may give clues to the formation scenario. Two features of ESPS are particularly interesting: the apsidal alignments and the large eccentricities. As e and ϖ are coupled, these two phenomena are likely the result of the same mechanism. There are two generic ways to pump up eccentricities: adiabatically, or impulsively, with respect to the secular timescale ($\gtrsim 10^5$ yr). Our variation of orbital elements provides a unique view into the effects of these mechanisms on the dynamics and stability of actual planetary systems. Several groups have examined this problem, and in this section we interpret our results in the context of theirs.

Of adiabatic scenarios a remnant planetary disk is the most likely candidate (Chiang & Murray 2002; Goldreich & Sari 2003). For at least the ν And system, a remnant disk external to planet d can provide a mechanism to pump up e_c and e_d to their current observed values (Chiang & Murray 2002). This method also predicts libration of Λ about 0, which is observed in this work. Conversely an impulsive force may also drive eccentricities to values significantly higher than zero (Malhotra 2002). The impulsive scenario also perturbs Λ . In adiabatic schemes the libration amplitude is small, whereas in impulsive cases it can be quite large ($> 45^\circ$). Throughout this paper we have shown configurations with libration amplitudes larger than 45° , i.e. Figs. 5 and 39, and smaller than 45° , i.e. Figs. 10, 31. This work therefore finds examples of systems which may result from either mechanism.

This impulsive scenario is difficult to reconcile with resonant systems. These systems most likely form as a result of resonance capture during the orbital migration epoch of planet formation (Snellgrove, Papaloizou, & Nelson 2001), which assumes adiabatic migration. This phenomenon seems qualitatively similar to the external disk model of Chiang & Murray. Their model, based on torques produced by Lindblad and corotation resonances, is very similar to planetary migration. However current orbital migration theory predicts that a Jupiter mass planet at 5AU in a plausible minimum mass solar nebula should migrate on a timescale of order 2500 years (Tanaka, Takeuchi, & Ward 2002) to 5000 years (Lufkin *et al.* 2003), which is a factor of 5 to 10 times shorter than the typical secular timescale for planetary systems. This suggests the planetary disk model might actually be impulsive, but only marginally so. However Lufkin *et al.* also point out that the migration might be very impulsive in heavier disks. Understanding the rates of migration will be a major step toward resolving this issue of high eccentricities and apsidal alignment. All we can say now is that we are too limited in the number of resonant and interacting systems to determine if their eccentricities result from similar processes.

The results presented here, coupled with Malhotra (2002) support the theory that the eccentricities of planets in interacting systems result from planet-planet scatterings. This possibility has been investigated substantially (Rasio & Ford 1996; Ford, Havlickova, & Rasio 2001; Weidenschilling & Marzari 2002; Malhotra 2002). The proximity of these systems to the

Table 13 - The Stability of Planetary Systems

| System | R | τ (10^5 yr) | N_{good} | f_{stable} | f_1 | f_2 | f_3 | f_4 |
|------------|------|---------------------|------------|--------------|-------|-------|-------|-------|
| GJ876 | 2.03 | 0.47 | 950 | 0.056 | 0.04 | 0.96 | - | - |
| HD82943 | 2.01 | 3.4 | 955 | 0.188 | 0.09 | 0.91 | - | - |
| 47UMa | 2.38 | 8.4 | 997 | 0.803 | 0.00 | 1.00 | - | - |
| Gas Giants | 2.48 | 33.2 | 996 | 0.857 | 0.00 | 0.14 | 0.24 | 0.62 |
| Jup-Sat | 2.48 | 33.2 | 992 | 0.963 | 0.07 | 0.93 | - | - |
| v And | 5.4 | 10 | 996 | 0.861 | 0.07 | 0.54 | 0.39 | - |
| HD168443 | 30.5 | 13.6 | 1000 | 1.0 | n/a | n/a | - | - |
| HD83443 | 9.99 | 0.023 | 847 | 1.0 | n/a | n/a | - | - |

edge of stability might imply that planet formation is an efficient process. Perhaps too efficient. As planets form, they are constantly perturbing each other with ever greater force. It is well known that ejections are common during planet formation. In fact some research predicts that the ejection of a fifth terrestrial planet may be needed to explain the period of heavy bombardment in the SS (Chambers, Lissauer, & Morbidelli 2001). So it is not too surprising that we find systems near instability because they form in an unstable state and eject massive bodies until they arrive in resonance, or reach the stability plateau. Some work has shown that if planet formation is very efficient (i.e. initially 10 Jupiter mass planets) then the subsequent scattering and ejections can produce distributions of a and e that are similar to those observed (Adams & Laughlin, 2003). Clearly this scenario is appealing, and will be verified in the next several years as simulations become more sophisticated and more multiple planet systems are detected.

Beyond the origin of large eccentricities and apsidal alignment, we find some inconsistencies in the theory of the origin of the very short period ($P \lesssim 10$ days) planets. As mentioned in §2 and §4.1, the effects of tidal circularization were not included in this model. For ν And the timescale for circularization is 80 million years (Trilling 2000), but we see that the eccentricity of ν And b can oscillate on 10^5 year timescales with an amplitude of 0.3. At this point it is unclear if the tidal damping will always overwhelm the perturbations of other companions. It could be that we have detected ν And b at a point in time in which its orbit is nearly circular. Perhaps we will discover planetary systems in which a close planet is being perturbed by external companions and the tidal circularization cannot compensate. However it seems more likely that the circularization is a stronger effect as we have yet to detect any planet inside the circularization radius on an eccentric orbit. Future numerical work should resolve this issue.

We observe that, in general, there is good agreement between our results and those performed with MEGNO. The sizes of stable regions appear to be overestimated in those papers, but that is most likely due their choice for τ , usually 10^4 years. The shortcomings of MEGNO are most clearly demonstrated in the long term integrations of 47UMa. The top left of Fig. 38 shows a stable, but chaotic system which persists for 10^9 years. The uniqueness of systems such as this is unknown, but understanding the dynamics of chaotic, yet long-lasting, systems could yield new insights into planetary dynamics. Our own SS is another example of a system that displays weak chaos, yet can survive for very long periods of time (Laskar 1994).

This research is the first to examine the origin of high eccentricities and apsidal alignment with known systems. Most other work in this field is purely hypothetical. That type of research has the benefit of being unconstrained by statistics; they may integrate as many systems as they wish, with arbitrary initial conditions. This work, conversely, is the first attempt to coherently and consistently compare known systems in order to understand their dynamics and origins. At this point, with so few known systems, the two methods are complimentary, but as we discover more ESPS, the method described in this paper will become more valuable as it uses true ESPS as a starting point.

8. CONCLUSIONS

We have shown that this type of experiment can indeed constrain the observed orbital elements of planetary systems. Further we see that in almost all interacting and resonant systems

the current best fits to the system place them near the boundary between stability and instability. The fact that no system is completely unstable implies that the observations of these systems are reliable, and that the errors in the system are probably conservative. That is, all systematics have been removed, and statistical fluctuations are being overestimated.

Note that our estimates of the instability of these systems is in some sense an underestimate because of the possible presence of yet undetected lower mass companions. For example, it may turn out that 47UMa may have an undetected planet that would put it closer to the edge. On the other hand, the very existence of these systems shows that they are not unstable. As unsettling as it may be, it seems a large fraction of planetary systems, including our own, lie dangerously close to instability. As more and different types of systems are detected we will discover if all planetary systems are on the edge.

This method has shown that, dynamically, the SS is not a unique system. In fact, it lies in the middle stability category. Some systems lie nearer instability, others further. As the radial velocity searches continue, and astrometric searches begin, a SS analogue (circular orbits, large semi-major axes) will undoubtedly be discovered and we will finally be able to determine how the SS fits in with other planetary systems. But this experiment has shown that, with regards to its (close) proximity to unstable regions, the SS is a typical planetary system.

Recently more systems were announced; HD38529 (Fischer *et al.* 2003), a separated system, HD12661 (Fischer *et al.* 2003), an interacting system, and 55Cnc a 3 planet system with interior planets in 3:1 resonance and a distant companion (Marcy *et al.* 2002). The planets in HD38529 have masses less than HD168443, and comparable values for R , therefore it seems likely that they are fully stable. 55Cnc, however, might demonstrate different dynamics and edges as it is in a different mean motion resonance. Future planetary systems will most likely fall into the categories outlined in this paper. The results presented here suggest that f_{stable} for 55Cnc would lie between resonant and coupled systems. HD12661 is very similar to ν And, so we expect this system to show similar edges, probabilities, and dynamics.

Future work will address many of the issues brought up in §7. If planet formation is an efficient phenomenon, then we might suspect that additional companions lie in separated systems. Further we should be able to determine that the eccentricity distribution of ESPS result from a late scattering event. We also need to determine the origin of the edges presented here. A mathematical relationship probably exists which would make the classification of planetary systems trivial. The categories as defined here may be the result of small number statistics. Two systems, HD169830 and HD37124, in which $R \approx 10$ have been announced (Mayor *et al.* 2003, Butler *et al.* 2003). These system may reveal the boundary between interacting and separated systems. An analysis of these two systems and 55Cnc will help sharpen our classification of planetary systems.

Future work, both observational and theoretical, must address these issues. These systems as they are observed now reflect their histories, and hence provide us with the best path to unlocking the secrets of planet formation. As more and more observations of these planetary systems, additional planetary systems, and (hopefully) protoplanets are made, numerical studies such as this, and those cited here, should provide a deeper understanding of planet formation and dynamics.

9. ACKNOWLEDGMENTS

The authors wish to thank Chance Reschke for his help in completing these simulations. This manuscript was greatly clarified after an edit by Derek C. Richardson. We would also like to thank Renu Malhotra, and Nader Haghighipour for use-

ful discussions and suggestions. This work was funded by grants from NASA, NAI, and the NSF, and was simulated on computers donated by the University of Washington Student Technology Fund.

REFERENCES

- Adams, F.C., & Laughlin, G. 2003, *Icarus*, 163, 290.
 Barnes, R. & Quinn, T. 2001, *ApJ*, 550, 884
 Benedict, G.F. *et al.* 2002, *ApJ*, 581, L115
 Butler *et al.* 1999, *ApJ*, 526, 916
 Butler *et al.* 2002, *ApJ*, 578, 565
 Butler *et al.* 2003, *ApJ*, 582, 455
 Chambers, J.E., Lissauer, J.J., Morbidelli, A. 2001, *DPS*, #33.2309
 Chiang, E.I., Tabachnik, S., Tremaine, S. 2001, *AJ*, 122, 1607
 Chiang, E.I., Murray, N. 2002, *ApJ*, 576, 473
 Cincotta, P.M., & Simó, C. 2000, *A&AS*, 147, 205
 Duncan, M.J., Quinn, T., 1993 *ARA&A*, 31, 265
 Fischer *et al.* 2002, *ApJ*, 564, 1028
 Fischer *et al.* 2003, *ApJ*, 586, 1394
 Ford, E.B., Havlickova, M., Rasio, F.A. 2001, *Icarus*, 150, 303
 Gonzalez, G. 1998, *A&A*, 334, 221
 Gonzalez, G., & Laws, C. 2000, *AJ*, 119, 390
 Goldreich, S., & Sari, R. 2003, *ApJ*, 585, 1024
 Goździewski, K. 2002, *A&A* 393, 997
 Goździewski, K. & Maciejewski, A.J. 2001, *ApJ*, 563, L81
 Konacki, M. & Maciejewski, A.J. 1999, *ApJ*, 518, 442
 Laughlin, G., Adams, F.C. 1999, *ApJ*, 526, 881
 Laskar, J. 1994, *A&A*, 287, L9
 Laughlin, G., Chambers, J., & Fischer, D. 2002, *ApJ*, 579, 455
 Lecar, M., Franklin, F.A., Holman, M.J., & Murray, N.W. 2001, *ARA&A*, 39, 581
 Levison, H.F., & Duncan, M.J. 1994, *Icarus*, 108, 18
 Lissauer, J.J. 1993, *ARA&A*, 31, 129
 Lufkin, G. *et al.* 2003, *MNRAS*, in press
 Malhotra, R. 2002, *ApJ*, 575, L33
 Marcy, G.W. *et al.* 2001a, *ApJ*, 556, 296
 Marcy, G.W. *et al.* 2001b, *ApJ*, 555, 418
 Marcy, G.W. *et al.* 2002 *ApJ* 581 1375
 Marzari, F., Weidenschilling, S.J. 2002, *Icarus*, 156, 570
 Mayor, M. *et al.* 2003, *A&A* accepted, astro-ph/0310316.
 Michtchenko, T., & Ferraz-Mello, S. 2001, *AJ*, 122, 474
 Rasio, F.A., Tout, C.A., Lubow, S.H., Livio, M. 1996, *ApJ*, 470, 1187
 Rasio, F., & Ford, E. 1996, *Science*, 274, 954
 Rivera, E.J., & Lissauer, J.J. 2000, *ApJ*, 530, 454
 Rivera, E.J., & Lissauer, J.J. 2001a, *ApJ*, 558, 392
 Rivera, E.J., & Lissauer, J.J. 2001b, *ApJ*, 554, 1141
 Robutel, P., & Laskar, J. 2001, *Icarus*, 152, 4
 Santos, N.C., Israelian, G., Mayor, M. 2000, *A&A*, 363, 228
 Snellgrove, M.D., Papaloizou, J.C.B., Nelson, R.P. 2001, *A&A*, 374, 1092
 Stepinski, T.F., Malhotra, R., Black, D.C. 2000, *ApJ*, 545, 1044
 Sussman, G.J., & Wisdom, J. 1988, *Science*, 241, 433
 Sussman, G.J., & Wisdom, J. 1992, *Science*, 257, 56
 Tanaka, H., Takeuki, T., & Ward, W.R. 2002, *ApJ*, 565, 1257
 Trilling, D.E. 2000, *ApJ*, 537, L61.
 Varadi, F., Ghil, M., & Kaula, W.M. 1999, *Icarus*, 139, 286